TR 9

OPHIOLITES, VOLCANOES, TURBIDITES, AND ACTIVE TECTONICS OF THE WESTERN TRANSVERSE RANGES/SOUTHERN COAST RANGES

CSUN Department of Geological Sciences
27th Annual Fall Field Frolic
August 20-22, 2009

Leaders: Doug Yule and Dick Heermance

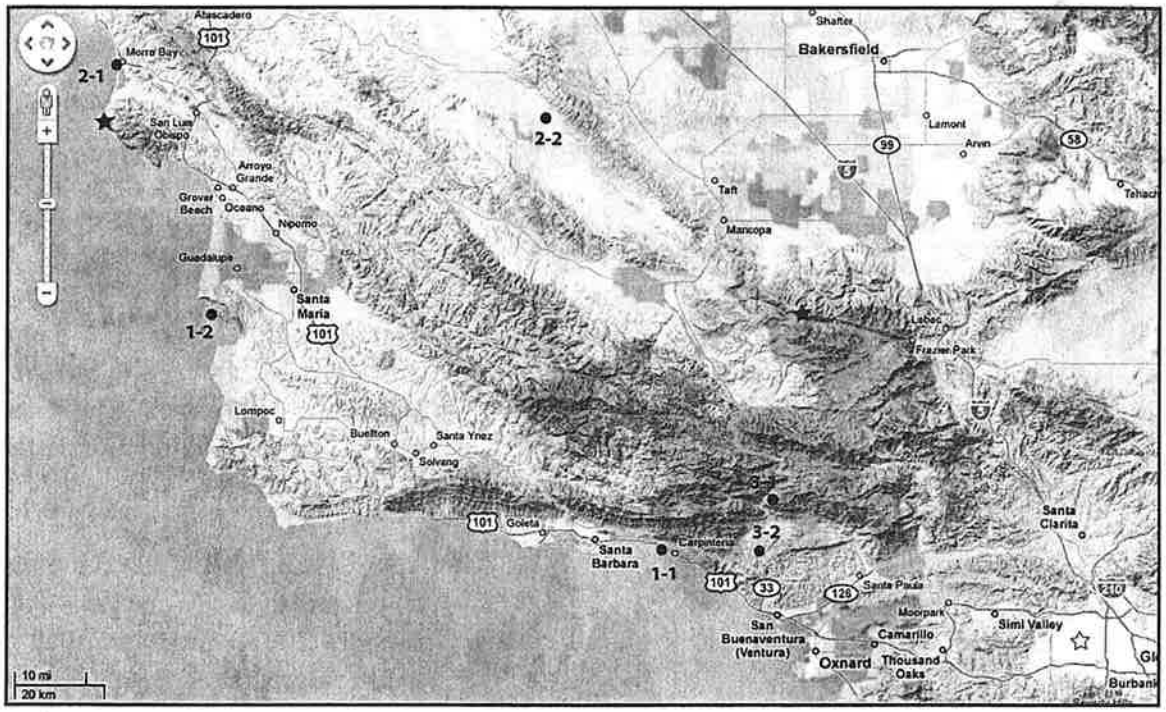

Itinerary:
Day 1 Loon Point Fault (1-1) and Pt. Sal ophiolite (1-2)
Day 2 Morro Rock (2-1) and Carrizo Plain (2-2)
Day 3 Wheeler Gorge (3-1) and Lake Casitas (3-2)

Stars denote campgrounds (Montana de Oro State Park on west, Marial Campground on east)

(1-1)

Stop 1 (Thursday, August 20): **Loon Point Fault**

Location: beach at Padaro Ln and 101 just east of Santa Barbara, CA

The Loon Point fault is a south-dipping, oblique-thrust fault that strikes east-west and is part of tthe east-west trending Santa Barbara fold-and-thrust belt. Along the beach at Loon Point, the fault is exposed and places the terrestrial Pleistocene Casitas Formation and overlying ~105 ka marine terrace deposits over the marine Santa Barbara Formation and overlying alluvium. The hanging wall strata and overlying terrace surface are deformed into an anticline above the fault.

Stratigraphy of the Ventura Basin (Keller, 1995)

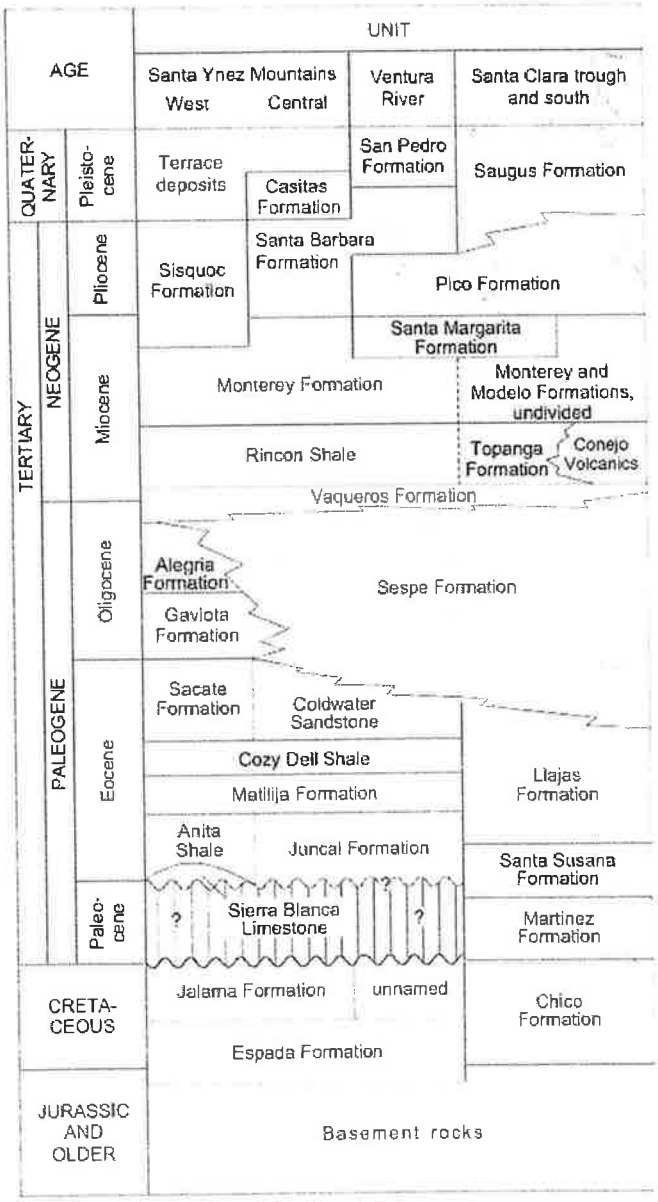

REFERENCES:

Keller, 1995. Ventura basin province (013). *In*: National Assessment of United States Oil and Gas Resources – Results, Methodology, and Supporting Data (eds Gautier D, Dolton GL, Takahashi KI, Varnes KL), U.S. Geological Survey Digital Data Series 30, CD-ROM, Reston, VA.

Minor S.A., K.S. Kellogg, R. G. Stanley, L. D. Gurrola, E. A. Keller, and T. R Brandt, 2007, Geologic map of the Santa Barbara Coastal Plain Area, Santa Barbara County, CA, USGS Publication.

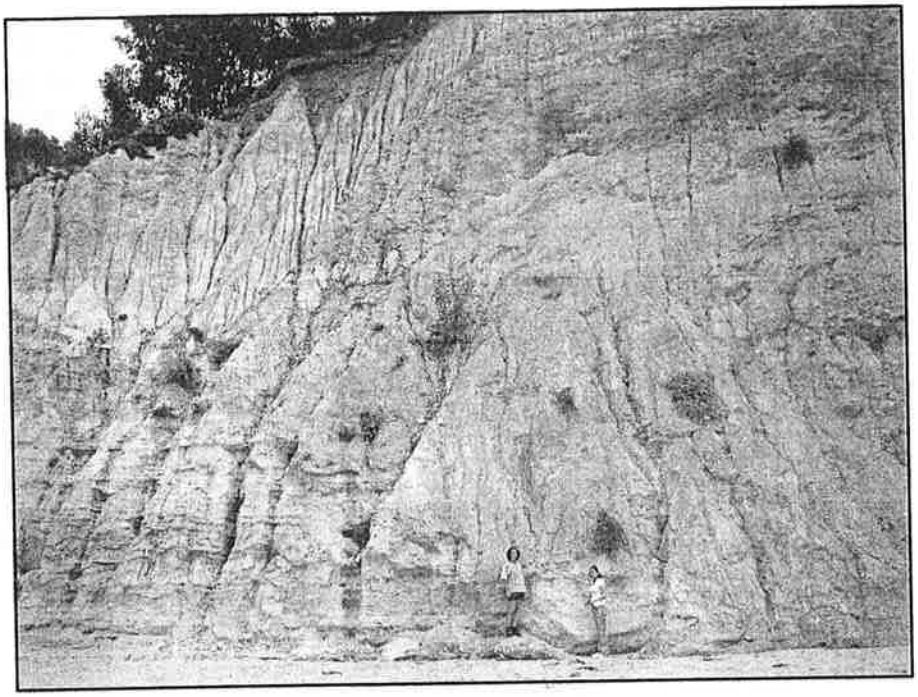

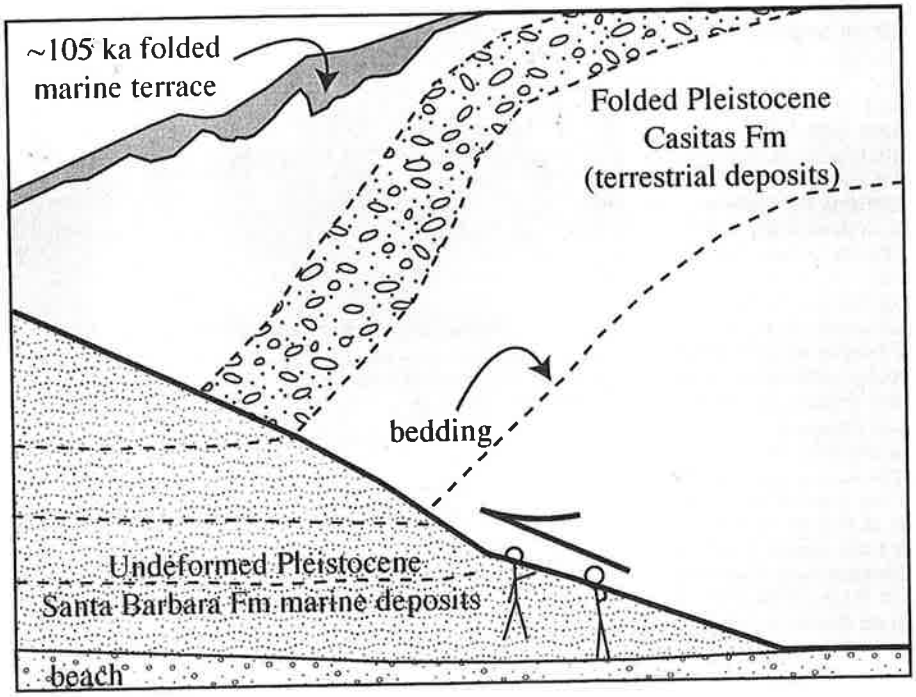

Photo and geologic interpretation of the Loon Point Fault near Santa Barbara. View is to the north. Photo by R. Heermance. Geology is from Minor et al., 2007.

Stop 4 1-2

Vol. 6, No. 2 February 1996

GSA TODAY

A Publication of the Geological Society of America

INSIDE

Alternate Origins of the Coast Range Ophiolite (California): Introduction and Implications

William R. Dickinson, Department of Geosciences, University of Arizona, Tucson, AZ 85721

Clifford A. Hopson, Department of Geological Sciences, University of California, Santa Barbara, CA 93106

Jason B. Saleeby, Division of Geological and Planetary Sciences, California Institute of Technology, Pasadena, CA 91125

ABSTRACT

Correctly interpreting the tectonic evolution of the California continental margin requires understanding the origin of the Jurassic Coast Range Ophiolite, which represents a fragment of mafic-to-ultramafic crust of oceanic character lying depositionally beneath the western flank of the Great Valley forearc basin in fault contact with the Franciscan subduction complex of the California Coast Ranges. Three contrasting hypotheses for genesis of the ophiolite as seafloor are each based on internally consistent logic within the framework of plate tectonics, but are mutually exclusive and lead to strikingly different interpretations of regional tectonic relations, even though each assumes that the Sierra Nevada batholith to the east represents the eroded roots of a magmatic arc linked to subduction along the Mesozoic continental margin. To encourage the further work or analysis needed to develop a definitive interpretation, summary arguments for each hypothesis of Coast Range Ophiolite genesis in mid- to late Jurassic time are presented in parallel: (1) backarc spreading behind an east-facing intraoceanic island arc that then collided and amalgamated with the Sierran continental-margin arc; (2) paleoequatorial mid-ocean spreading to form oceanic lithosphere that was then drawn northward toward a subduction zone in front of the Sierran continental-margin arc; and (3) forearc spreading within the forearc region of the Sierran continental-margin arc in response to transtensional deformation during slab rollback.

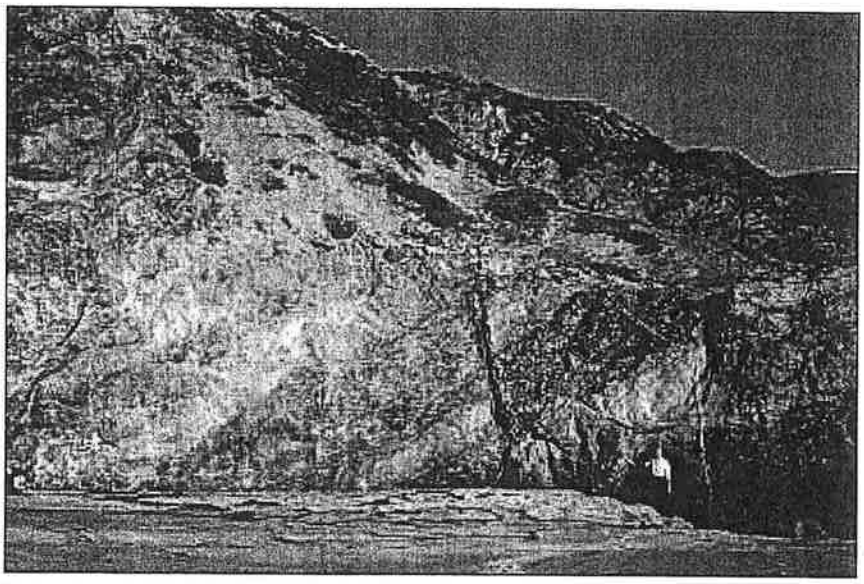

Multiple basaltic sills of the sheeted dike and sill complex, Point Sal remnant of the Middle Jurassic Coast Range ophiolite. The ridge in background exposes sheeted sills and (to left of tree on the skyline) base of the overlying pillow lavas.

INTRODUCTION

Widely distributed exposures of the Jurassic Coast Range Ophiolite in the California Coast Ranges represent deformed and structurally dismembered segments of oceanic crust and uppermost mantle now incorporated within the continental block (Bailey et al., 1970). The overall span of Middle to Late Jurassic radiometric ages for igneous components of ophiolite and postophiolite hypabyssal intrusions is ~170 to 155-150 Ma (Hopson et al., 1981, 1991; Saleeby et al., 1984; Mattinson and Hopson, 1992). Understanding correctly the origin and emplacement of the Coast Range Ophiolite is essential for understanding the Mesozoic evolution of the Cordilleran continental margin (Saleeby, 1992). The time is long past when geoscientists could assume that all ophiolites formed in the same way or have the same tectonic significance.

With the help of co-authors, we outline here three divergent views on the origin of the Coast Range Ophiolite. We emphasize that our areas of agreement are larger than our area of disagreement. We each interpret the Coast Range Ophiolite layered assemblage as a profile of mafic crust and lithosphere of oceanic character, and we infer that this profile was formed through magmatism induced by mantle upwelling linked to lithospheric extension or "spreading." We each also argue for emplacement of the ophiolite within the conceptual framework of plate tectonics, taking the Sierra Nevada composite batholith to the east to be the deeply eroded roots of Jurassic-Cretaceous magmatic arc belts, and regarding Franciscan rocks of the California Coast Ranges farther west as part of the subduction complex accreted near the trench that was paired with the Sierran-Klamath arc assemblage

Ophiolite *continued on p. 2*

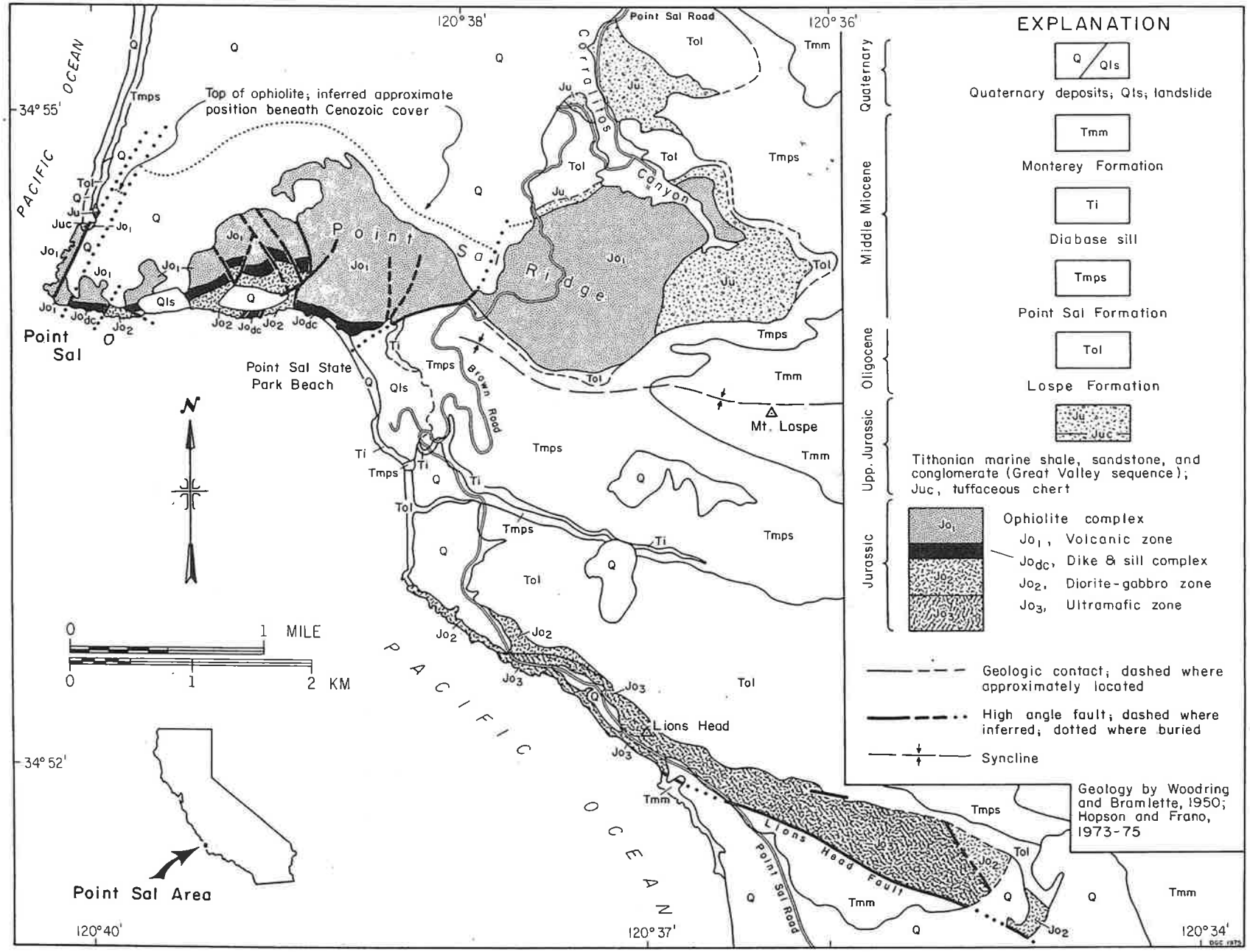

Figure 1. Geologic map of the Point Sal area, Santa Barbara County, California.

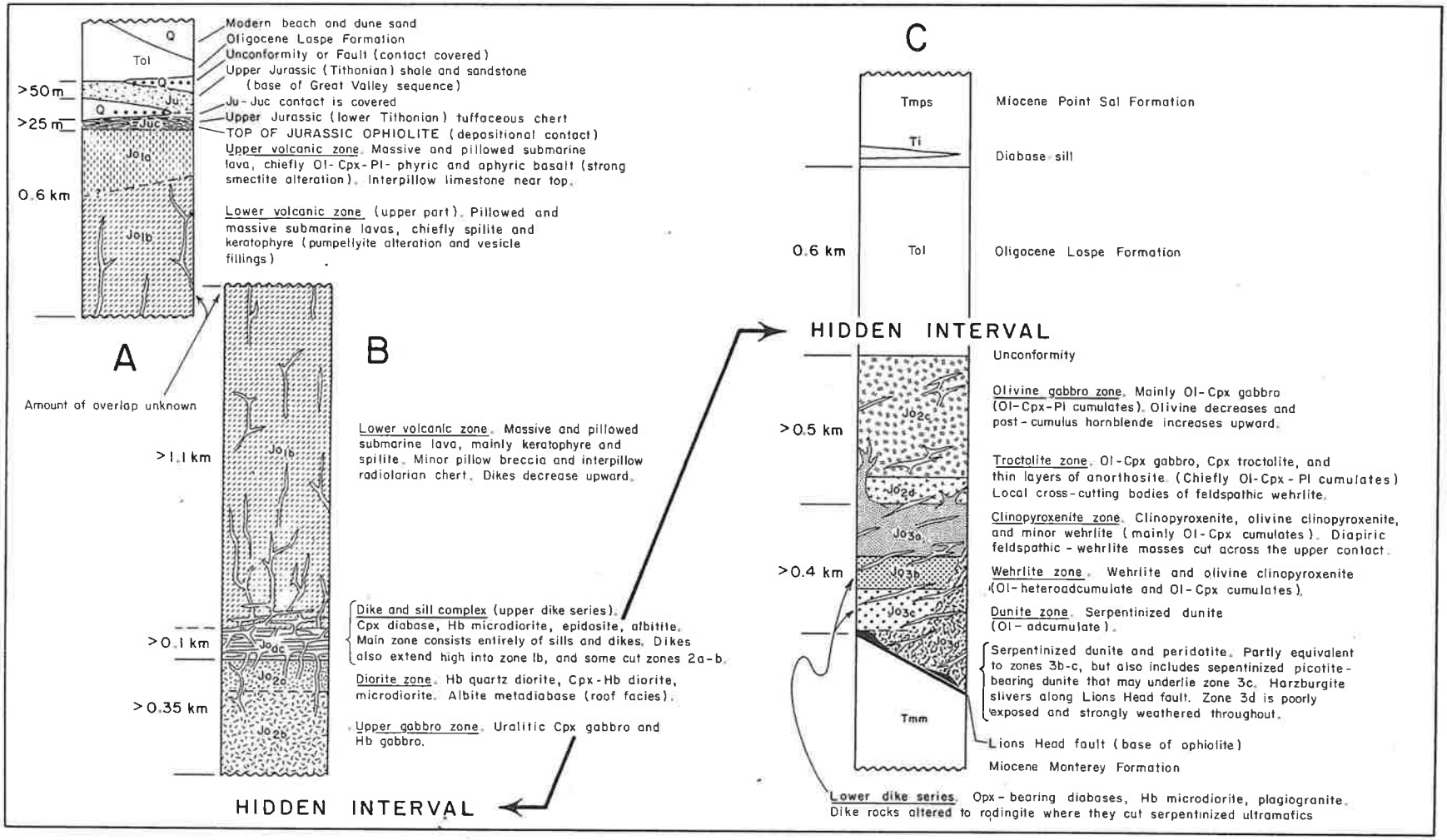

Figure 2. Columnar sections: A, coastal strip extending north from Point Sal (Fig. 10); B, Point Sal Ridge, northwest and north of Point Sal State Park Beach (Fig. 3); C, Lions Head-Point Moritto area (Fig. 5)

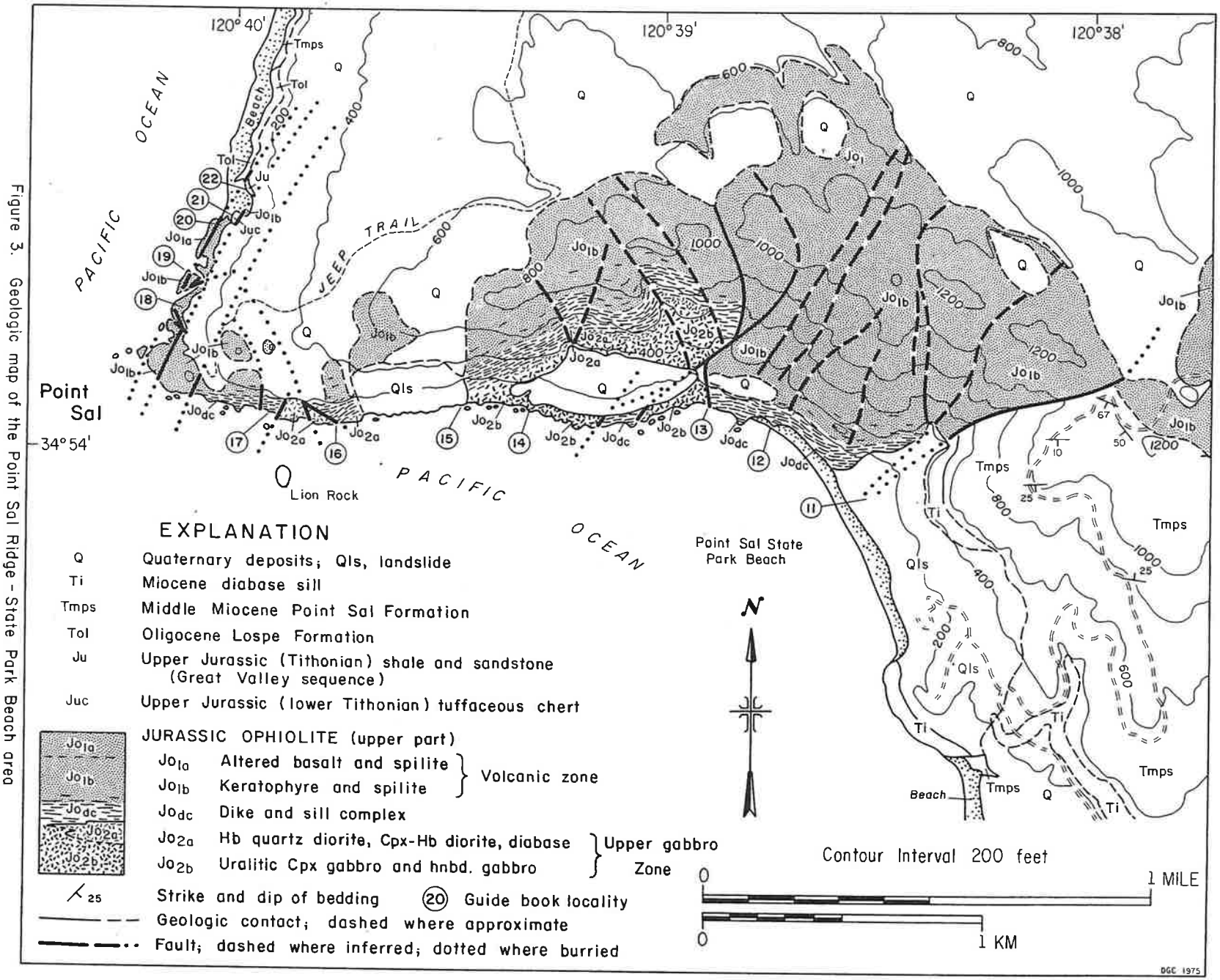

Figure 3. Geologic map of the Point Sal Ridge - State Park Beach area

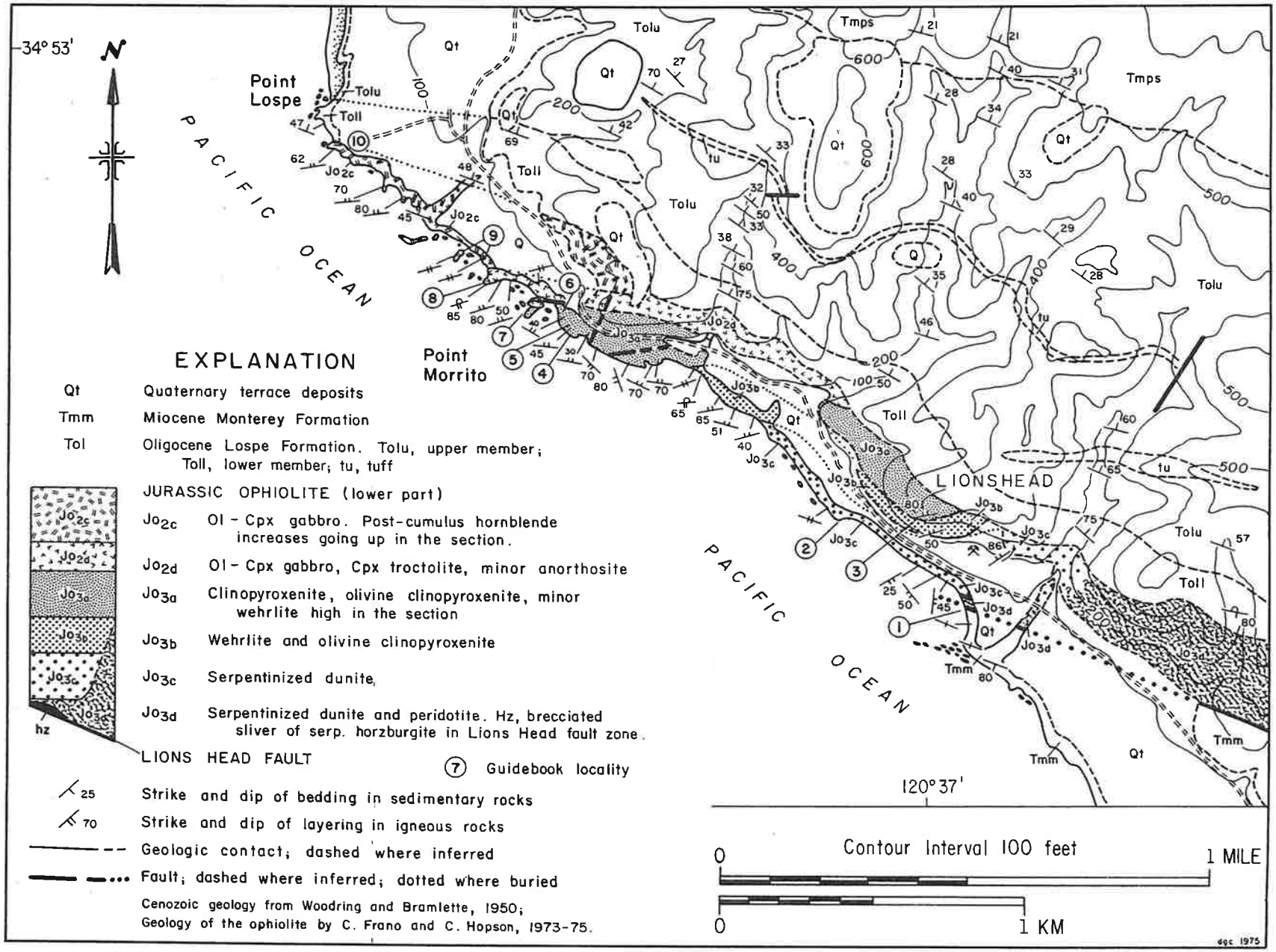

Figure 5. Geologic map of the Lions Head - Point Morrito area

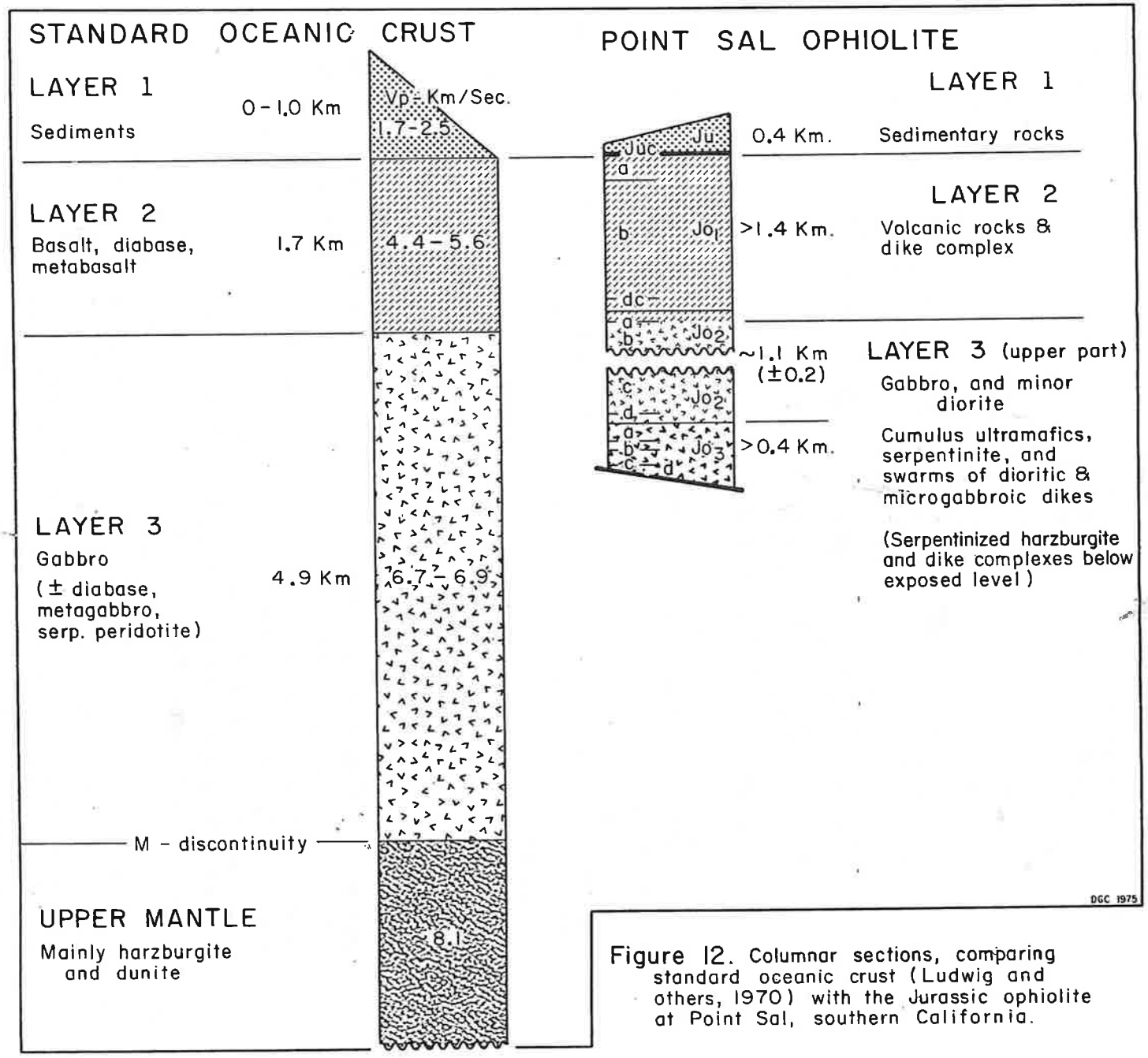

Figure 12. Columnar sections, comparing standard oceanic crust (Ludwig and others, 1970) with the Jurassic ophiolite at Point Sal, southern California.

The "basement" terrane here in coastal San Luis Obispo County is the Mesozoic age Franciscan Assemblage. The Franciscan rocks are fascinating. Their designation as an "assemblage" or "mélange" used here and elsewhere in literature reflects both the complexity and unique genesis of these rocks. The Franciscan assemblage is a collection of whole and dismembered ophiolite (ocean crust and mantle) that formed at a spreading ridge and accreted to the continent along the leading edge of a subduction zone. Rock exposures include graywacke sandstone, shale and chert mixed with basalt and occasional blocks of conglomerate, exotic blue schist and serpentinite. These rocks were accreted tectonically to California during Mesozoic and early Cenozoic subduction of the Farallon Plate (Figure 2).

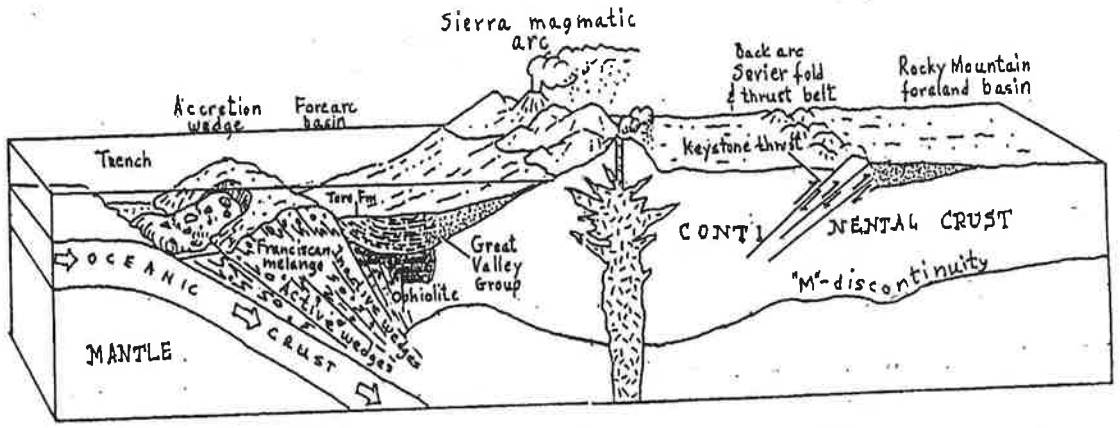

Figure 2. Schematic block diagram depicting the western edge of North America during Mesozoic time. The accretion wedge at the leading edge of the continent represents the Franciscan assemblage or mélange exposed in the Coast Ranges today. Tectonic shearing along with submarine landslides mix and deform the accreted material resulting in a complex mixture of dismembered ocean crust and mantle. (Artwork by D.D. Trent after Page 1972, and Dott and Prothero 1994)

Both intruding and overlying the Franciscan assemblage are Cenozoic age rocks that formed as a consequence of the changing tectonic regime during the onset of transform shear along the San Andreas Fault. A chain of mid-Cenozoic (Miocene) volcanic necks known locally as the Morros or seven sisters, intrude the Franciscan. Extrusive equivalents to these dacitic plugs are recognized in discontinuous exposures north and east of Cambria and in the Los Osos Valley near Morro Bay. Minor amounts of volcanic rocks are intercalated within sediments that unconformably overlie the Franciscan basement. The sediments range from deep marine siliceous shales and turbidite sandstones, to fossiliferous, nearshore deposits, nonmarine terrace sands and gravels that in turn are overlain by Pleistocene and younger eolian dune sand. Marine units within the Cenozoic strata reflect localized pull-apart basin fill associated with the development of the San Andreas transform.

Late Pliocene to Holocene deformation is reflected in the modern topography and is expressed by folding, and by reverse and right-lateral faulting seen throughout the central coast. (Figure 3) Interplay between Pleistocene sea level change and tectonic uplift has stranded numerous marine terraces throughout the region. Recent earthquakes in the area attest to the continuing tectonic activity.

(Stop 2-1)

to these hypabyssal intrusions are located in scattered exposures along Los Osos Valley, near Cambria and approximately 15km. east of Cambria (Ernst and Hall 1974).

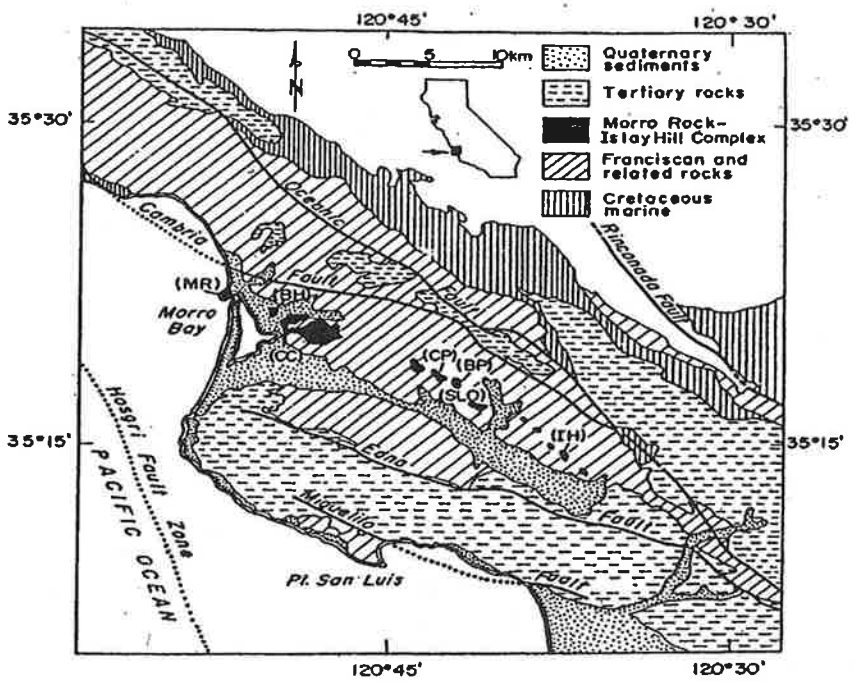

Figure 4. Generalized geology depicting principle rock units and location of the Morro Rock – Islay Hill intrusive complex or The Morros".

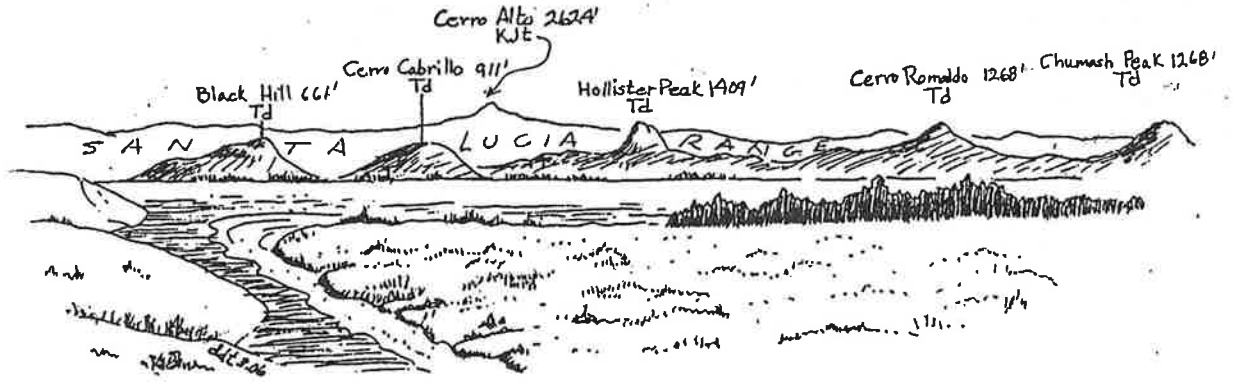

Figure 5. View to the northeast from the Morro Dunes sand spit showing the Morro Bay estuary and five of the Morros. Td = Miocene dacite, Kjt = Upper Jurassic-Lower Cretaceous Torro formation . (Sketch by Dee Trent)

Morro rock and associated peaks are composed of dacite and rhyodacite and all exposures within the suite exhibit distinct porphyritic texture. The pronounced linear trend of the peaks strongly suggests that a fault or joint system controlled the position and form of the pluton during emplacement. It is likely that each peak represents the tip of a series of intrusive fingers that bled off a more expansive, tabular-shaped pluton that intruded the Franciscan assemblage.

seismic potential can be measured. With these data, Hansen and others estimate an uplift rate for this portion of the San Luis Range of approximately 0.06 to 0.23 m/kyr., for the past 120 ka. This rate is comparable to regions in California characterized by strike-slip faulting, but is considerably less than maximum rates of 3 to 5 m/kyr south of the Mendocino Triple Junction or 5 to 7 m/kyr for areas characterized by crustal shortening such as the Ventura Anticline.

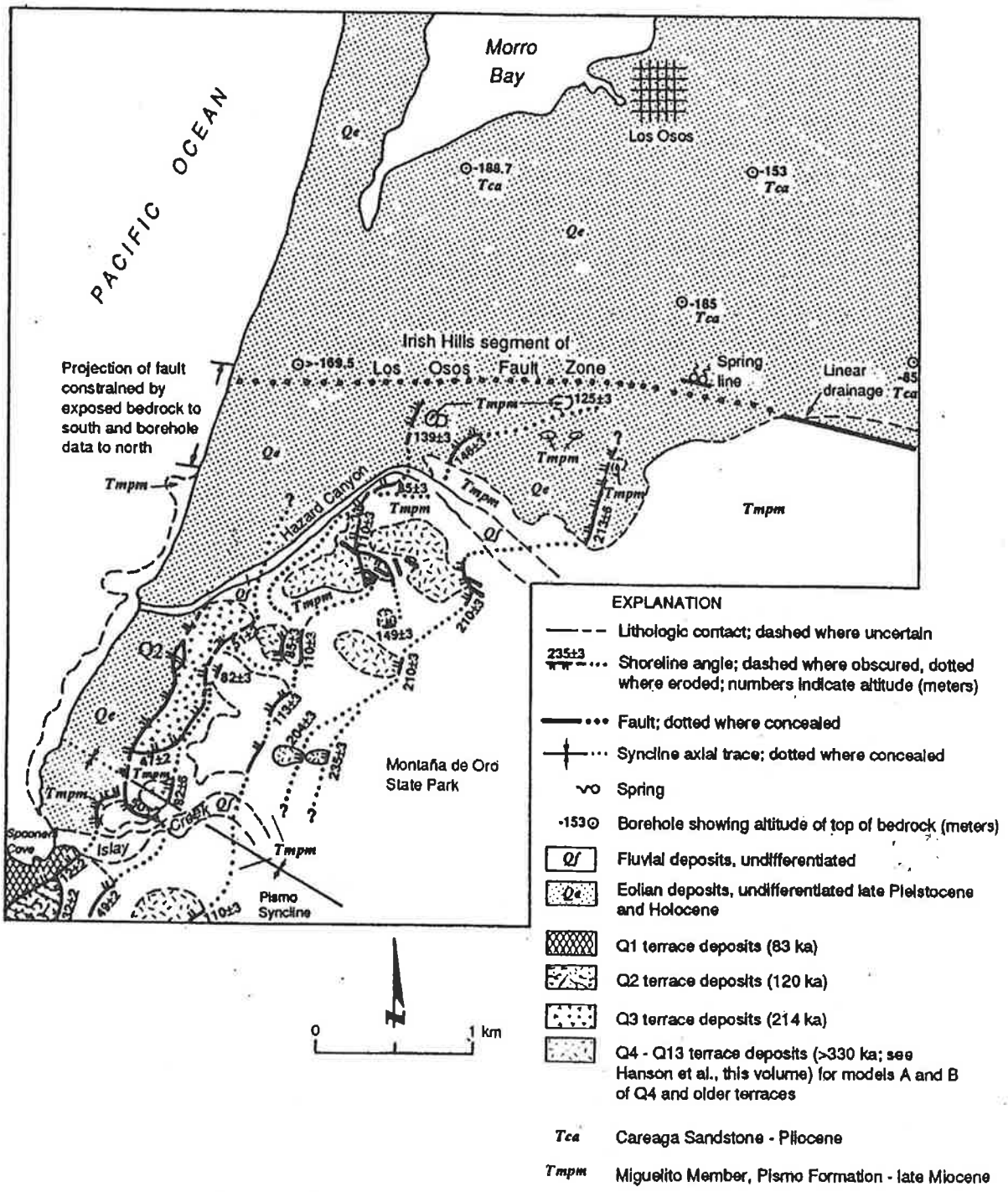

Figure 8 Generalized geologic map of Quaternary deposits of the Montana de Oro and Morro bay areas illustrating distribution of marine terraces and interpreted location of the Los Osos fault zone. (Lettis and Hall 1994)

While the uplift rates here may not rival those of highly active tectonic regimes, they are significant and worthy of discussion. Regional mapping, geodetic and seismologic studies show that this area is experiencing northeast-directed crustal shortening (Lettis and others, 2004). Structural folds observed in the Miguelito shale place a limit on the initiation of this deformation. The earliest compression must post date deposition of the youngest rocks within these Tertiary sediments. Apparently, by middle Pliocene, the basin into which the Miguelito formation formed, was experiencing compression, folding, and uplift. By the Pleistocene the folding had ceased, but not the compression as the area continues to rise as a block along thrust faults that bound the northern and southeastern edges of the San Luis range (Figure 3, 8 and 9). These faults, the Los Osos on the north side and the Wilmar Avenue (and others) on the southeast side are controlling the uplift of the range as a more-or-less intact unit. The ongoing deformation is believed to reflect the clockwise rotation of the western Transverse Ranges. This movement shortens the crust by pushing the south-central Coast Ranges against the relatively stable buttress of the Salinian block to the north (Lettis and others 2004).

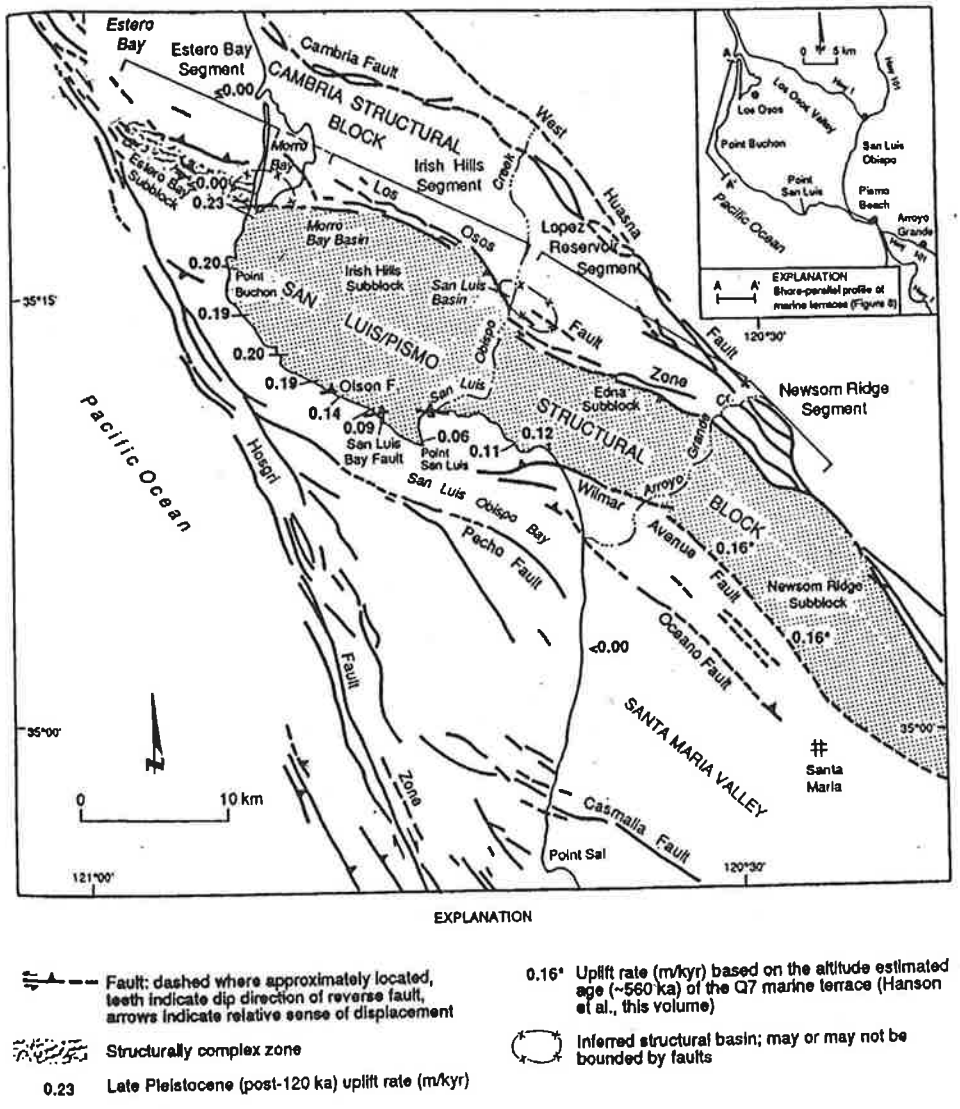

Figure 9. Regional map showing the San Luis/Pismo Structural Block Range and principal bounding faults for the San Luis Range (From Lettis and Hall, 1994)

EVALUATION OF THE DECEMBER 22, 2003 M_W 6.5 SAN SIMEON EARTHQUAKE

1.0 INTRODUCTION

On December 22, 2003 at 11:15 am PST a strong earthquake of magnitude (M_W) 6.5 struck the south-central coast region of California. The earthquake, called the San Simeon Earthquake, is located approximately 50 km NNW of Diablo Canyon, in the region 11 km northeast of San Simeon, at a depth of about 11.3 km. This is the largest earthquake to occur in the San Simeon region since the 1952 Bryson Earthquake of magnitude (M_L) 6.2, approximately 8 km north of the 2003 epicenter. The San Simeon Earthquake was widely felt from Los Angeles to San Francisco, including the PG&E General Office complex at 245 Market St. Earthquake ground effects include landslides and related ground failure near the epicenter, however, no surface faulting yet has been observed. Most of the damage occurred in Paso Robles, 39 km ENE of the epicenter; two deaths have been confirmed due to a building collapse. The earthquake was strongly felt in the Administration Building at Diablo Canyon Power Plant; no damage was reported at the plant.

This article contains information about the San Simeon earthquake that is primarily from PG&E's final report to the U.S. Nuclear Regulatory Commission, dated December 2004 (PG&E Letter DCL-04-177). At the end of the article (after the reference section) we include updates on the San Simeon earthquake sequence from our current seismicity study which we hope to publish in 2006.

The main shock initiated rupture at depth to the southeast and triggered a vigorous aftershock sequence that extends about 30 km southeast of the main shock. As of December 26, 2003 approximately 960 aftershocks have occurred, including 17 M 4 earthquakes. As of November 16, 2004, the USGS online database (USGS, 2004) reported over 8000 aftershocks greater than about magnitude 0.5. During the first 24 hours the aftershock activity was about 50% higher than the average for a California sequence (USGS online report, December 24, 2003). Two items of interest are; 1) one of the M4 aftershocks occurred on Oct 2, 2004, just 5 days after the M6.0 Parkfield earthquake of September 28, 2004, and 2) no M5 aftershocks have occurred to date.

The San Simeon earthquake was a reverse fault event beneath the Santa Lucia Mountains. It occurred along a NW-SE trending fault plane that dips either to the SW or NE. This is a common fault mechanism along this trend (McLaren and Savage, 2001).

2.0 TECTONIC FRAMEWORK

The San Simeon earthquake occurred in a region of transpressional deformation associated with the boundary between the Pacific Plate and the Sierran microplate (Figure 2-1). Our characterization of the tectonic setting of the region is based upon extensive geologic mapping and analyses of seismicity performed over the past 18 years (for example, PG&E, 1988, 1991;

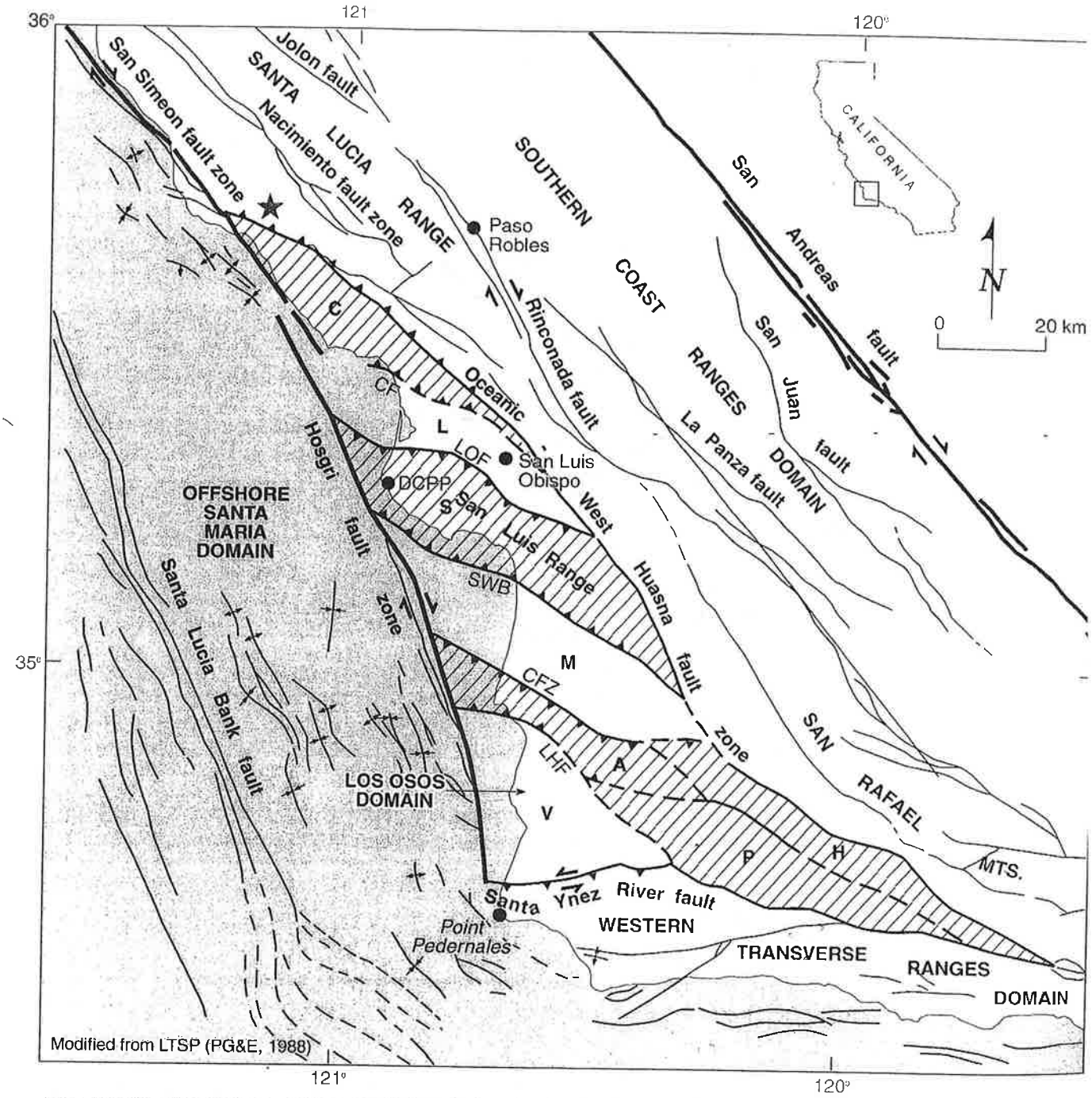

Note: Los Osos domain (incorporating areas that are hachured and colored yellow) is bounded by the Hosgri fault zone, Oceanic-West Huasna fault zone, and the Santa Ynez River fault. The Los Osos domain is divided into distinct structural blocks, including: C-Cambria, L-Los Osos Valley, S-San Luis/Pismo, M-Santa Maria Valley, A-Casmalia, H-Solomon Hills, V-Vandenberg/Lompoc, P-Purisima. Hachured areas show location of Quaternary uplift within the Los Osos domain. Bedrock and Quaternary faults shown as light lines; domain boundary faults shown as bold lines. CF = Cayucos fault, LOF = Los Osos fault, SWB = Southwest Boundary zone; CFZ = Casmalia fault zone; LHF = Lion's Head fault. DCPP = Diablo Canyon Power Plant. Red star shows location of the December 2003 San Simeon earthquake.

Figure 2-3. Major kinematic domains in west-central California.

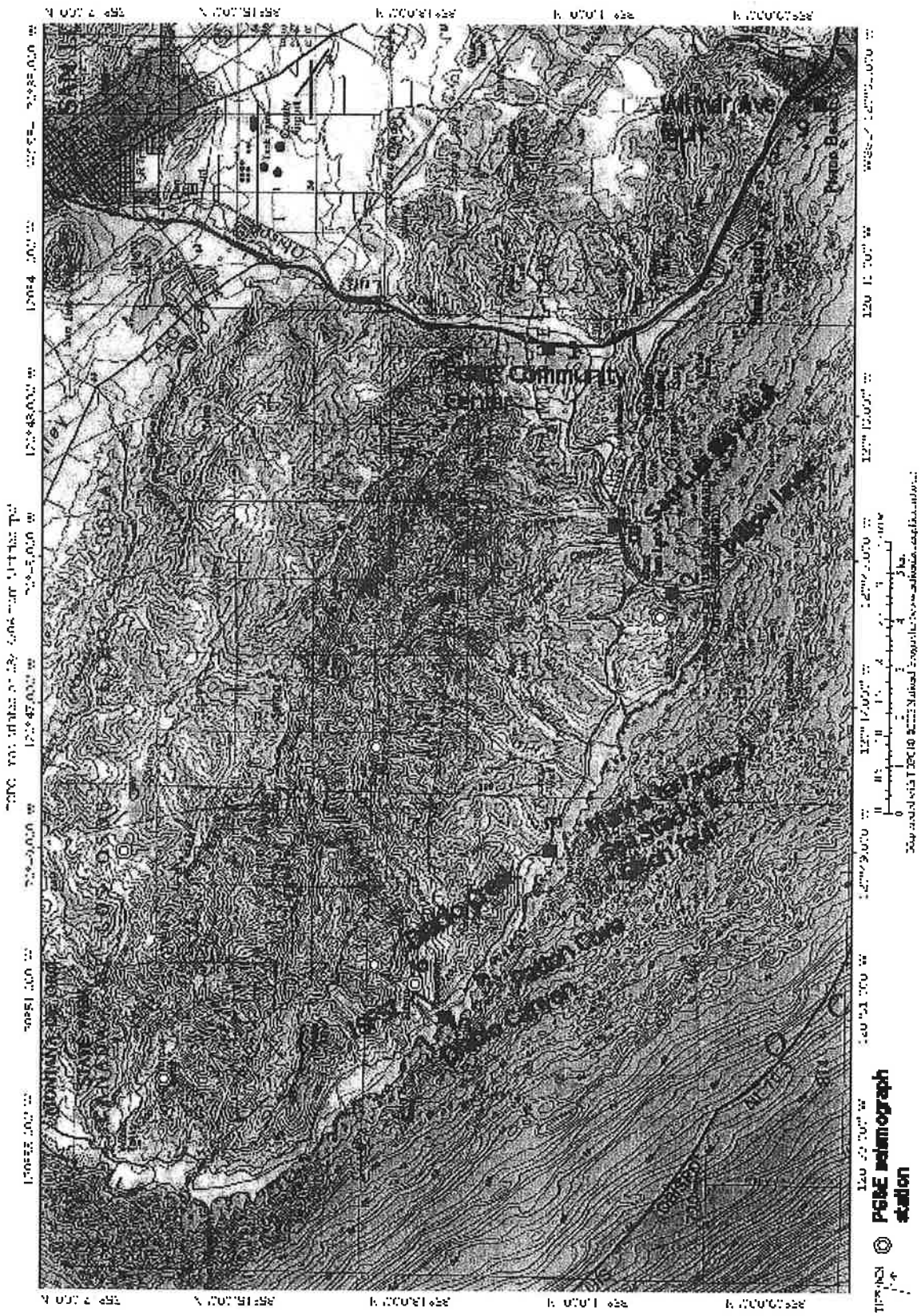

NAGT Field Trip stops – Day 3

16

2-2

Bulletin of the Seismological Society of America. Vol. 68, No. 5, pp. 1421–1448, October 1978

SLIP ALONG THE SAN ANDREAS FAULT ASSOCIATED WITH THE GREAT 1857 EARTHQUAKE

By Kerry E. Sieh*

ABSTRACT

Historical records indicate that several meters of lateral slip along the San Andreas fault accompanied the great 1857 earthquake in central and southern California. These records, together with dendrochronological evidence, suggest that the rupture occurred along 360 to 400+ km of the fault, including several tens of kilometers of the currently creeping reach in central California.

Geomorphic expressions of late Holocene right-lateral offsets are abundant along the 1857 rupture. Along 300 kilometers of the 1857 rupture, between Cholame and Wrightwood, the youngest discernible offset ranges from 3 to 9½ meters. Dormancy of the fault since 1857 almost certainly indicates that this latest offset was created in 1857.

Fault slip apparently associated with the 1857 earthquake varies in a broadly systematic way along the trace of the fault. It is relatively uniform along each of several long segments, but changes rather abruptly in value between these segments. This nonuniform displacement pattern may imply that some segments of the fault rupture more frequently or experience a slower long-term slip rate than others.

The 1857 offsets indicate a seismic moment, m_o, between 5.3 and 8.7 × 10^{27} dyne-cm, assuming a 10- to 15-km depth of rupture and relatively uniform slip as a function of depth. A comparison with the rupture length, average slip value, and tectonic setting of the California earthquake of 1906 ($M_S = 8\frac{1}{4}$) indicates a value of $M = 8\frac{1}{4}+$ for the 1857 event.

Introduction

The California earthquake of January 9, 1857 is one of the great historic earthquakes of the western United States. Contemporary accounts indicate that it was produced by several meters of sudden lateral slip along the south-central reach of the San Andreas fault and was felt over at least 350,000 km^2 (Figure 1). A majority of reports indicate that the duration of the earthquake was between 1 and 3 min.

The dormancy of the south-central reach of the fault since 1857 has prompted suggestions that past and future slip along this reach might well be characterized by great 1857-type events separated by long intervals of dormancy (Allen, 1968). A comparative study of the amount of fault slip associated with the 1857 and earlier events along the south-central reach of the fault would provide a test of the above hypothesis. Such a comparison depends, of course, upon a knowledge of the 1857 fault slip. The acquisition of this knowledge is therefore the major concern of this paper. A forthcoming paper and Sieh (1977, Ch. 2) compare 1857 and earlier slip events.

Wood (1955) has dealt with most of the sparse historical data available for assessing the size of 1857 offsets. A small amount of additional historical information is presented herein. The main body of this paper, however, is devoted to the presentation and geomorphic analysis of the small channel offsets which form the basis for estimating the size and extent of the 1857 offsets.

* Present address: Division of Geological and Planetary Sciences 170-25, California Institute of Technology, Pasadena, California 91125.

17

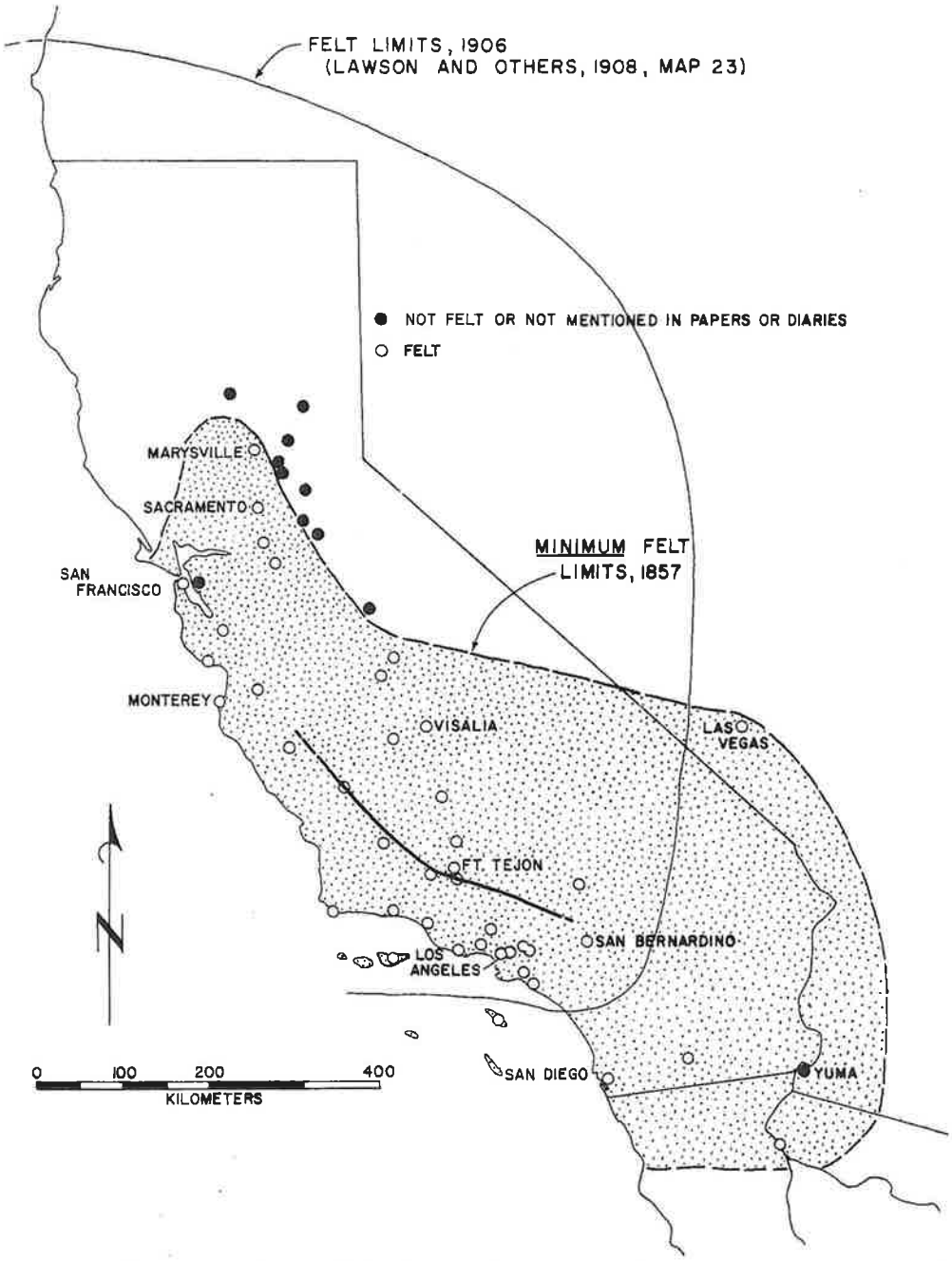

FIG. 1. Felt reports of the great 1857 earthquake (from Agnew and Sieh, in press) and the segment of the San Andreas fault which slipped to produce the earthquake.

BACKGROUND

Extent of surface faulting associated with the 1857 earthquake. Several first- and second-hand contemporary accounts of surface fractures (Wood, 1955) leave little doubt that the great 1857 earthquake was produced by strike slip along at least the 230-km reach of the San Andreas fault from Cholame Valley to Lake Elizabeth (Figure 2). Two later accounts suggest that surface faulting may have occurred as

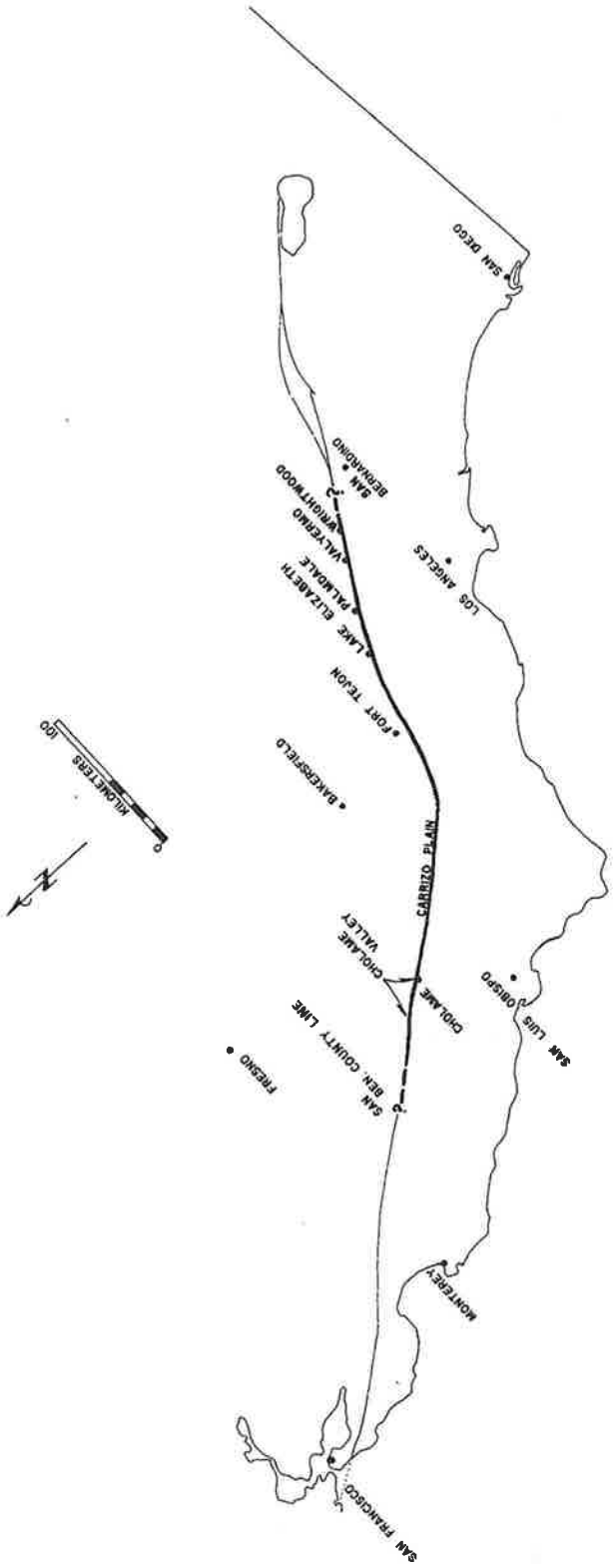

FIG. 2. Extent of fault rupture associated with the 1857 earthquake. The segment of the fault which has been creeping during the period of historical record extends from Cholame to a point northeast of Monterey.

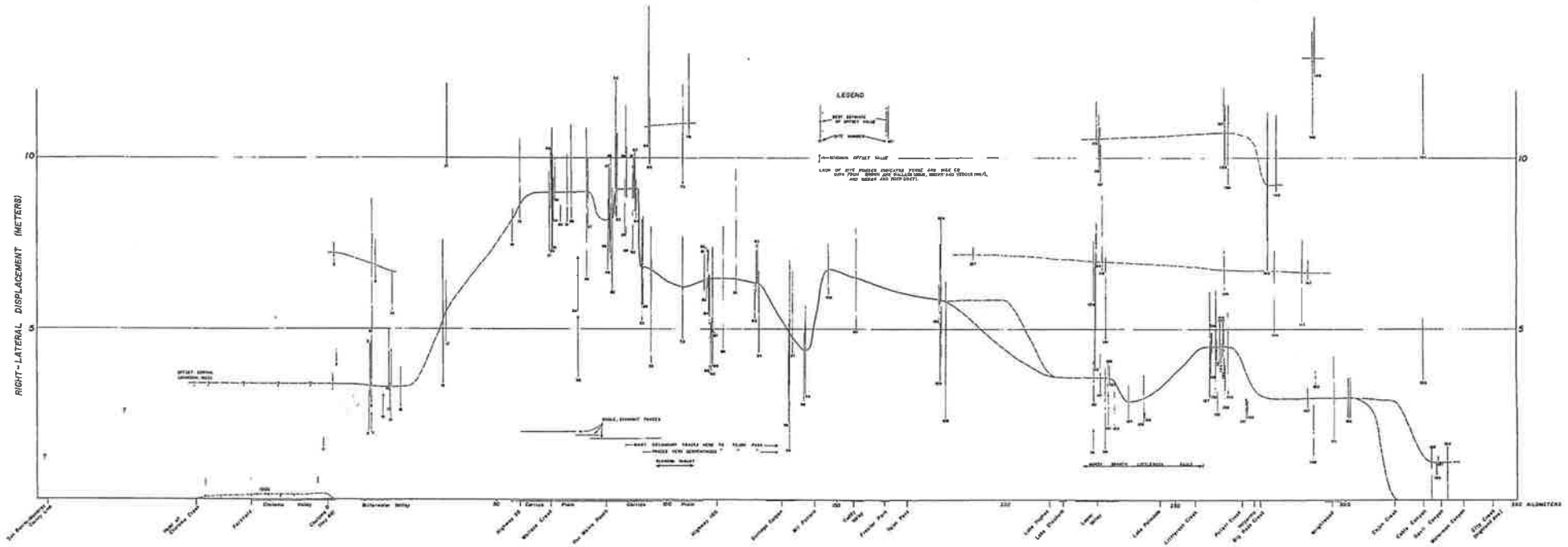

FIG. 1. Smallest offsets along the south-central reach of the San Andreas fault, believed to represent fault slip associated with the 1857 earthquake. Location along the fault is plotted on the horizontal axis. The offsets associated with the $M_L = 5.5$ 1952 Parkfield-Cholame earthquake, shown near the left (northwestern) side of the diagram, provide a remarkable contrast to the large 1857 offsets.

Bulletin of the Seismological Society of America, Vol. 68, No. 6, pp. 1731–1749, December 1978

CENTRAL CALIFORNIA FORESHOCKS OF THE GREAT 1857 EARTHQUAKE

By Kerry E. Sieh

ABSTRACT

Analysis of contemporary accounts indicates that several small to moderate central California earthquakes preceded the great 1857 earthquake by 1 to 9 hr. The earliest events apparently were felt only in the San Francisco area or the Sacramento and Sierran Foothills region. Two later and much more widely felt foreshocks were experienced within the region bounded by San Francisco, Visalia, Fort Tejon, and Santa Barbara. A comparison with felt areas and intensity distributions of modern events of known source and magnitude indicates that these later two shocks were $5 \leqq M \leqslant 6$ and probably originated at some point within an area of radius ≈60 km that includes the southeastern 100 km of the historically creeping segment of the San Andreas fault. The northwestern terminus of the 1857 rupture is probably located along this segment.

If the location of these foreshocks is indicative of the epicenter of the main event, then the several-hundred-kilometer main-event rupture propagated principally in a unilateral fashion toward the southeast. This implies that, like many great earthquakes, the 1857 rupture originated on a fault segment historically characterized by moderate activity and propagated into an historically quiet segment.

There is a strong possibility that the foreshock activity represents a moderate Parkfield-Cholame sequence similar to those of 1901, 1922, 1934, and 1966. To the extent that such premonitory activity is characteristic of the failure of the 1857 segment of the fault, studies of the creeping segment of the fault may be relevant to the prediction of large earthquakes in central and southern California.

Introduction

One intriguing aspect of many contemporary accounts of the great California earthquake of January 9, 1857 is the mention of shocks felt during the several hours prior to the main earthquake. If indeed these were foreshocks, their location might indicate the epicentral region of the main shock (Kelleher and Savino, 1975; Dewey, 1976). Knowledge of the approximate epicenter of the main shock would enable calculation of more realistic models of strong ground motion for the earthquake and for similar future events (R. Butler and H. Kanamori, personal communication). Predicted long-period motions in Los Angeles, for example, are more severe if the 1857 rupture is modeled to begin near its northwestern terminus and propagate southeastward toward the city than if it is modeled to begin east of Los Angeles near San Bernardino and propagate to the northwest.

Documentation of foreshocks to the main 1857 event is also important in the context of earthquake prediction, especially if such precursory activity commonly precedes 1857-like events.

In this paper the evidence for precursory events is critically analyzed and interpreted. The data base is drawn from many contemporary accounts, all of which are published on microfiche in Agnew and Sieh (this volume). In this paper I refer to these accounts by number, as listed in their Table 1.

Timekeeping in California in 1857

The seismic activity of the night and early morning prior to the main shock (~8:24 a.m.) is restricted to west-central California by the distribution of earthquake reports.

Figure 1 and Table 1 summarize the times and places the shocks were felt. Determining to what degree the variation in reported times of this activity is due to inaccurate and imprecise timekeeping is critical to the interpretation of the activity. It will be shown that if substantial inaccuracies and imprecision are assumed, moderately large early-morning shocks can be postulated. If, on the other hand, the reported times are strictly accepted, one can only conclude that most of central California began to pop with a series of small local events prior to the main shock.

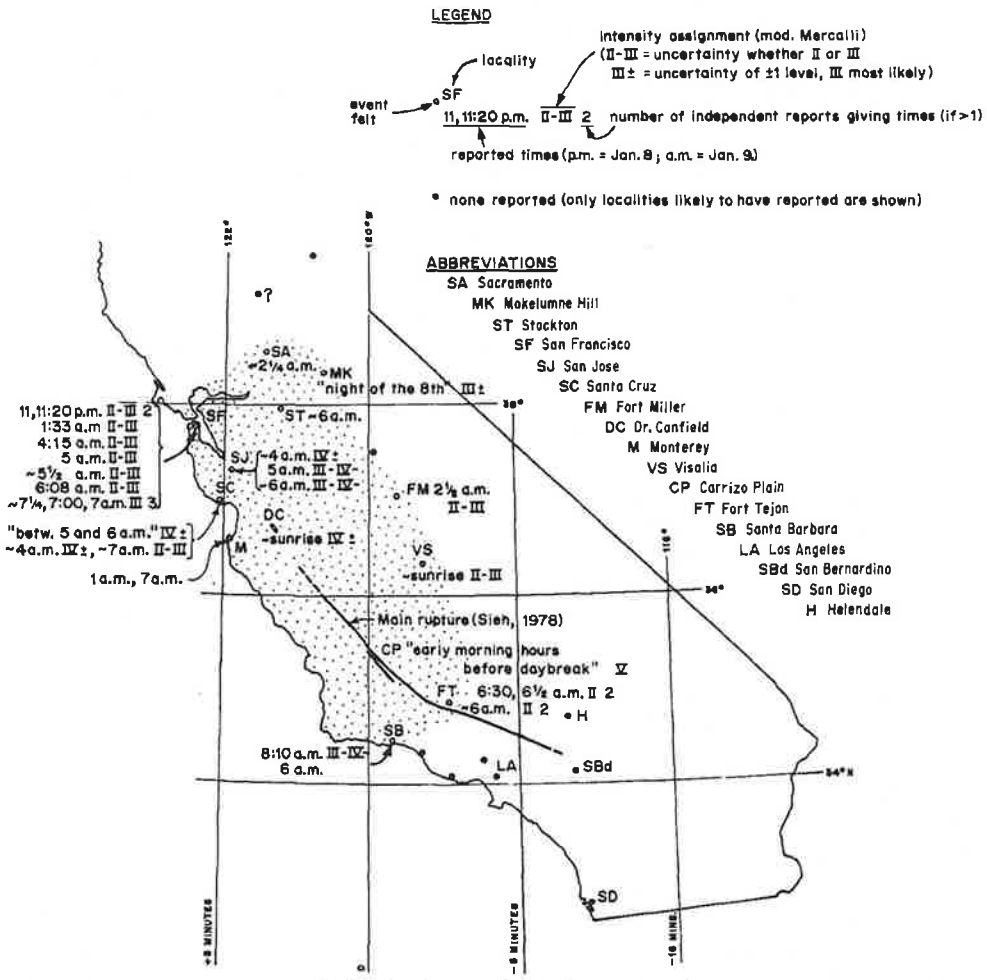

FIG. 1. Reports of shocks felt during the hours prior to the great earthquake of 9 January 1857 (08:24 PST) come from many localities within central California (*stippled region*). The great variety of times reported certainly indicates the occurrence of several shocks, but is due in part to poor timekeeping and to the use of local, rather than standard, time in 1857. The difference between local time and Pacific Standard Time is shown as a function of longitude.

The analysis that follows demonstrates that substantial imprecision and, in some cases, inaccuracy in the reports must be taken into account in interpreting the data.

Precision of individuals' accounts. In several cases, it is clear that the witness or reporter of an earthquake was not concerned with precise reporting of the time the event was experienced. For example, Mr. Canaday, an expressman from Ft. Tejon, reportedly told the Stockton *Daily Argus* (57) that a light shock was felt at Ft. Tejon at "about 6" a.m., whereas he reportedly told the Stockton *San Joaquin*

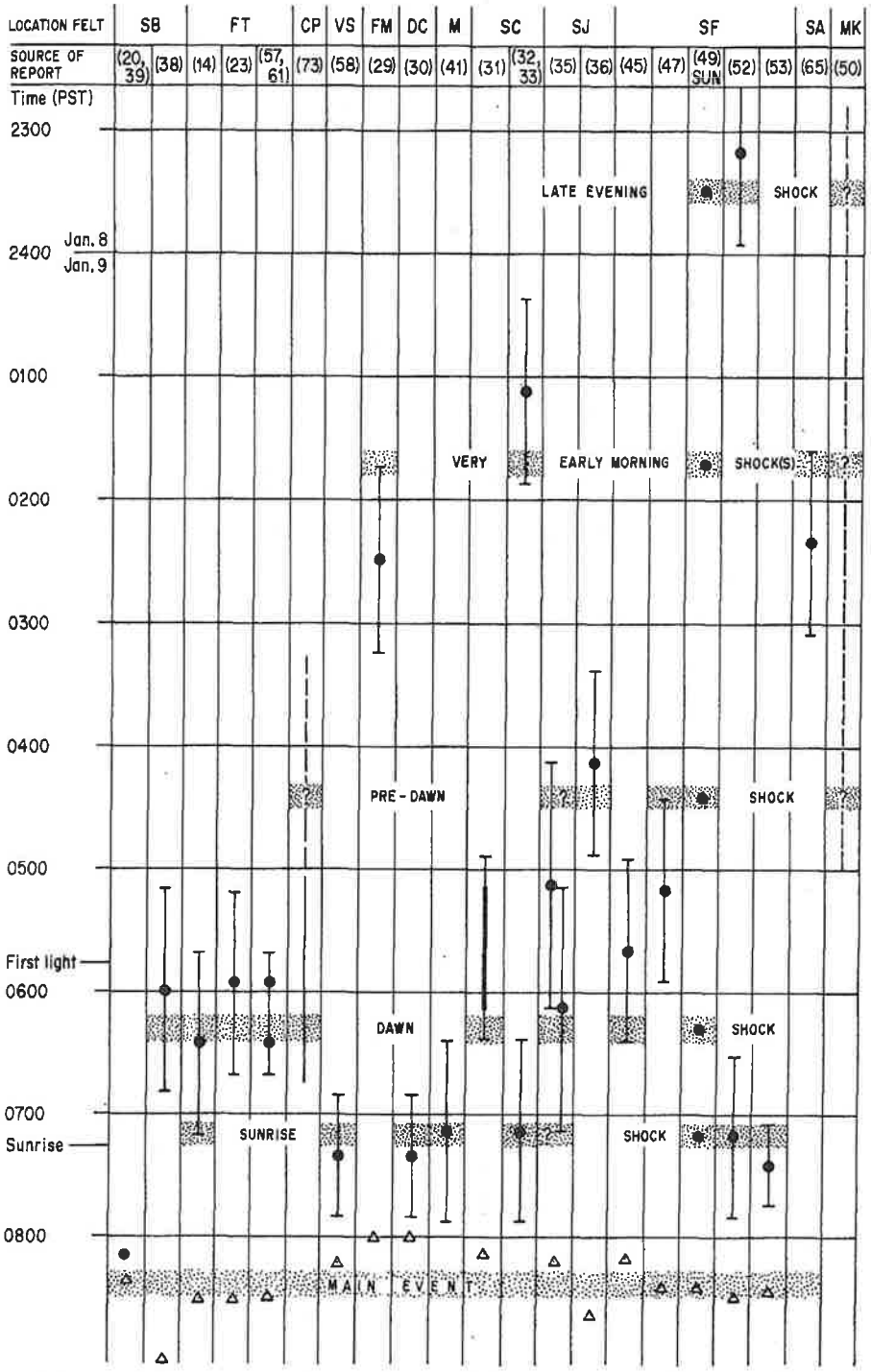

FIG. 2. Reported times of shocks felt at various localities corrected to Pacific Standard Time (PST). Error bars are based upon a qualitative analysis of the precision of each account. At least five shocks seem to have occurred within 9 hr of the main shock. Abbreviations of localities are as in Figure 1 and numbers in parentheses refer to listing of accounts in Table 1 of Agnew and Sieh (1719, this volume).

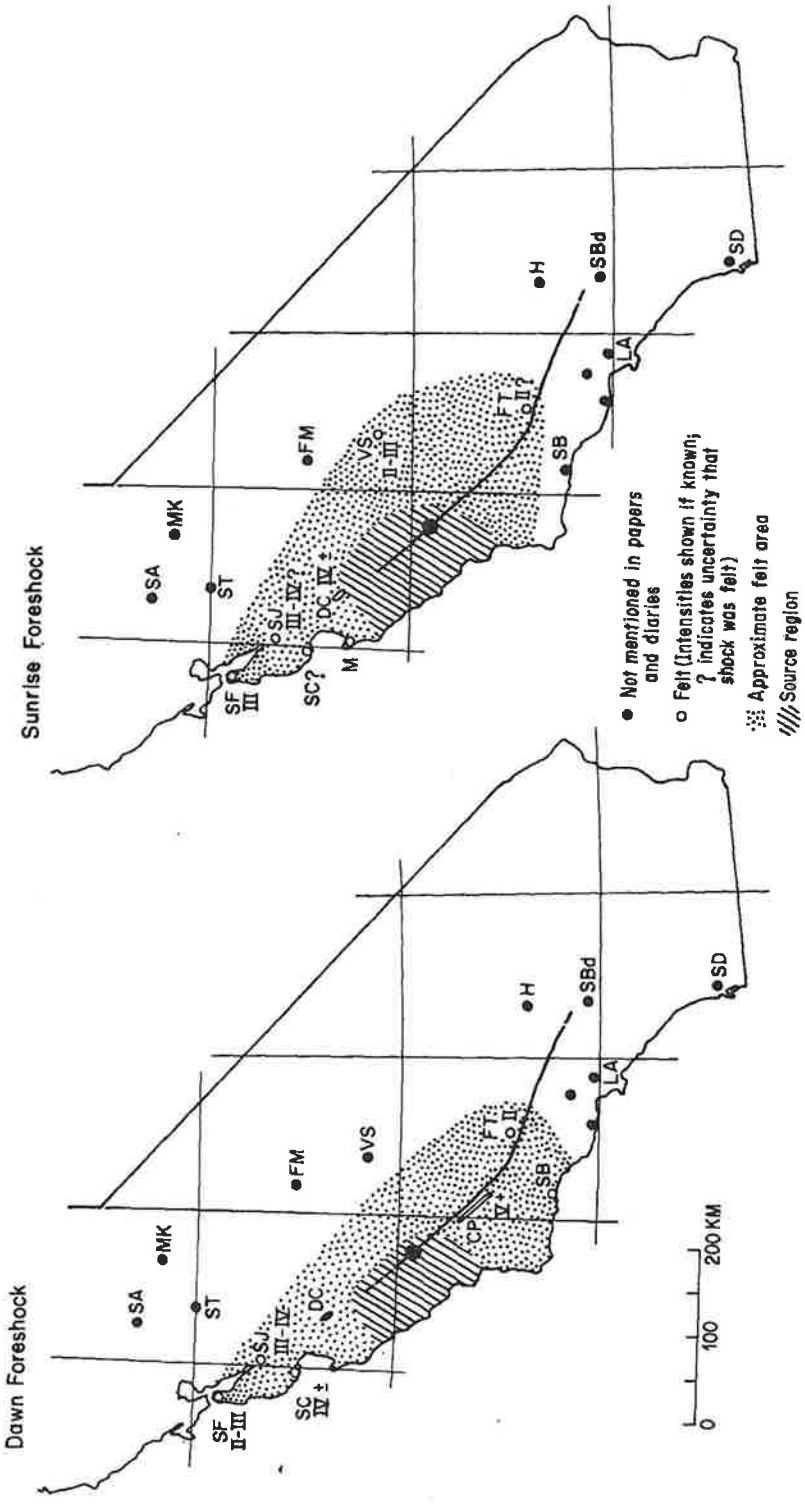

FIG. 3. Felt reports and source regions of the Dawn and Sunrise foreshocks.

Holocene activity of the San Andreas fault at Wallace Creek, California

KERRY E. SIEH *Division of Geological and Planetary Sciences, 170-25 California Institute of Technology, Pasadena, California 91125*
RICHARD H. JAHNS* *School of Earth Sciences, Stanford University, Stanford, California 94305*

ABSTRACT

Wallace Creek is an ephemeral stream in central California, the present channel of which displays an offset of 128 m along the San Andreas fault. Geological investigations have elucidated the relatively simple evolution of this channel and related landforms and deposits. This history requires that the average rate of slip along the San Andreas fault has been 33.9 ± 2.9 mm/yr for the past 3,700 yr and 35.8 + 5.4/-4.1 mm/yr for the past 13,250 yr. Small gullies near Wallace Creek record evidence for the amount of dextral slip during the past three great earthquakes. Slip during these great earthquakes ranged from ~9.5 to 12.3 m. Using these values and the average rate of slip during the late Holocene, we estimate that the period of dormancy preceding each of the past 3 great earthquakes was between 240 and 450 yr. This is in marked contrast to the shorter intervals (~150 yr) documented at sites 100 to 300 km to the southeast. These lengthy intervals suggest that a major portion of the San Andreas fault represented by the Wallace Creek site will not generate a great earthquake for at least another 100 yr. The slip rate determined at Wallace Creek enables us to argue, however, that rupture of a 90-km-long segment northwest of Wallace Creek, which sustained as much as 3.5 m of slip in 1857, is likely to generate a major earthquake by the turn of the century.

In addition, we note that the long-term rates of slip at Wallace Creek are indistinguishable from maximum fault-slip rates estimated from geodetic data along the creeping segment of the fault farther north. These historical rates of slip along the creeping reach thus do represent the long-term—that is, millennial—average, and no appreciable elastic strain is accumulating there.

Finally, we note that the Wallace Creek slip rate is appreciably lower than the average rate of slip (56 mm/yr) between the Pacific and North American plates determined for the interval of the past 3 m.y. The discrepancy is due principally to slippage along faults other than the San Andreas, but a slightly lower rate of plate motion during the Holocene epoch cannot be ruled out.

INTRODUCTION

California has experienced many episodes of tectonic activity during the past 200 m.y. During the past 15 m.y. horizontal deformations due to the relative motion of the Pacific and North American plates have been dominant. On land, the major actor in this most recent plate-tectonic drama has been the San Andreas fault, across which ~300 km of right-lateral dislocation has accumulated since the middle Miocene (Hill and Dibblee, 1953; Crowell, 1962, 1981; Nilsen and Link, 1975).

The San Andreas fault traverses most of coastal California, running close to the populous Los Angeles and San Francisco Bay regions (Fig. 1a). Its historical record of occasional great earthquakes (Lawson and others, 1908; Agnew and Sieh, 1978) amply demonstrates that it poses a major natural hazard to inhabitants of these regions. The future behavior of the San Andreas fault thus has long been a topic of great interest to Californians. Interpretations of historical, geodetic, and geologic data have yielded estimates of one century to several centuries for the time between great earthquakes along the fault in the San Francisco Bay region (Reid, 1910; Thatcher, 1975). Geologic data indicate that similar recurrence intervals apply in southern California (Sieh, 1978b, and in press).

The behavior of the San Andreas fault during the past few thousands of years is one of the best clues to its future behavior. Useful forecasts concerning the likelihood or imminence of a great earthquake along the fault will be much more difficult without greater understanding of its behavior during the past several millennia.

In this paper, we present and discuss the geologic history of Wallace Creek, a locality about halfway between San Francisco and Los Angeles that contains much information about the Holocene behavior of the San Andreas fault (Fig. 1a). For the purpose of determining rates of slip in Holocene time, the channel of Wallace Creek offers excellent possibilities. The channel crosses and is offset along a well-defined, linear trace of the San Andreas fault in the Carrizo Plain of central California (Fig. 1b). It is relatively isolated from other large drainages, and, therefore, its history is not complicated by involvement with remnants of other drainages that have been brought into juxtaposition.

The simple geometry of Wallace Creek suggests a simple history of development. Arnold and Johnson (1909) inferred 120 m of offset on the San Andreas fault, because the modern channel of the creek runs along the fault for about that distance. Wallace (1968) also inferred a simple history of offset involving incision of a channel into an alluvial plain, offset of ~250 m, then channel filling and new incision across the fault. The latest dextral offset of 128 m then accumulated. These interpretations are verified and quantified by us in this paper.

STRATIGRAPHY AND GEOMORPHOLOGY

Figure 2 is a geologic map of the Wallace Creek area that is based upon surficial mapping and study of sediments encountered in numerous excavations. The map shows four main geologic units: older fan alluvium (uncolored), younger fan alluvium (green), high-channel alluvium (dark orange), and low-channel alluvium (light orange). A mantle of slope wash and local alluvium, which is extensively burrowed by rodents, overlies most of the deposits. This unit has been mapped (brown) only where it is thicker than ~1 m and does not cover units and relationships that need to be shown on the map.

*Deceased.

Geological Society of America Bulletin, v. 95, p. 883–896, 11 figs., 3 tables, August 1984.

25

Figure 1. a. Wallace Creek (WC) is along the San Andreas fault (SAF) between Los Angeles (LA) and San Francisco (SF), in the Carrizo Plain of central California. b. This oblique aerial photograph shows the modern channel, which has been offset ~130 m, and an abandoned channel that has been offset ~380 m. An older abandoned channel, indicated by white arrow at left, has been offset ~475 m. Photograph by R. E. Wallace, 17 September 1974. View is northeastward.

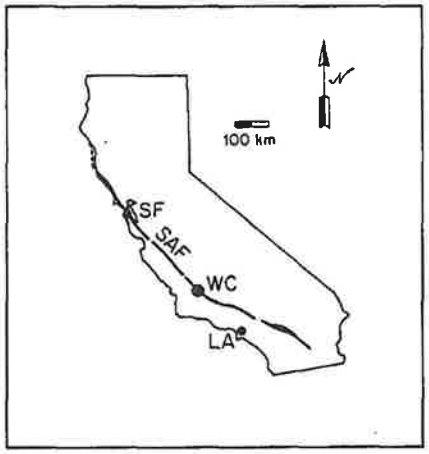

a

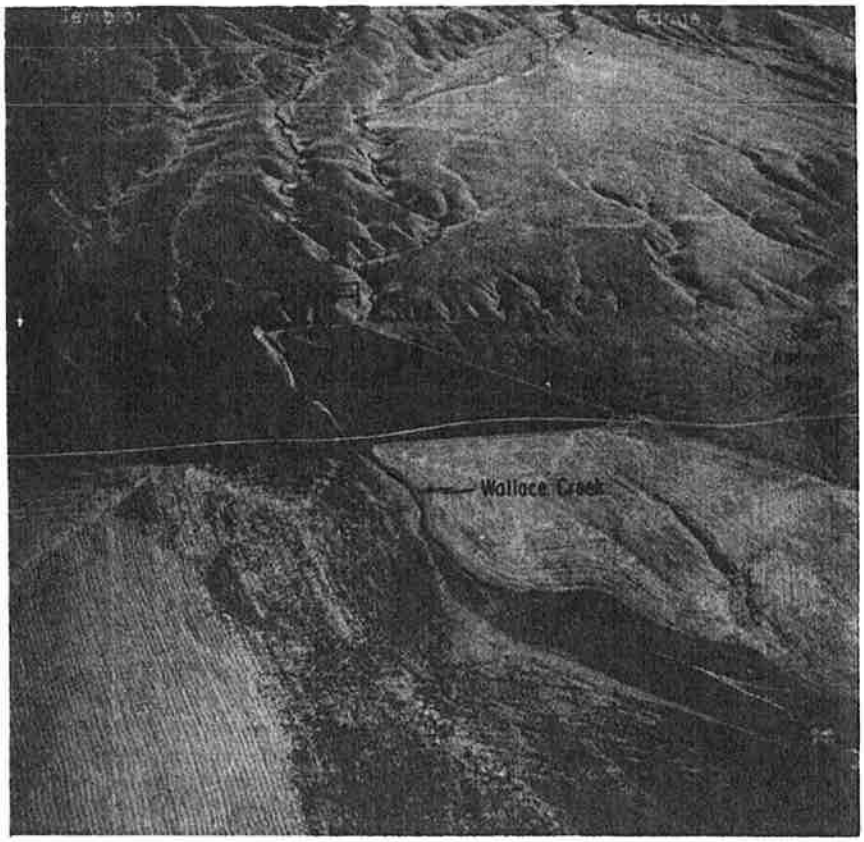

b

Older Fan Alluvium

Underlying all other units exposed at the site, there is a late Pleistocene alluvial fan deposit derived from the Temblor Range to the northeast. This deposit, here termed the "older fan alluvium," consists of thin sheets, lenses, and stringers of indurate silty clay, pebbly sandy clay, and sandy gravel. Most of the trenches (Figs. 2 and 3) exposed this unit. Southwest of the fault, the older fan alluvium is covered by various deposits, but northeast of the fault, the deformed fan surface is incised.

Charcoal disseminated within the older fan alluvium 4 m below the surface of the fan in trench 5 (Fig. 3), yielded an age of 19,340 ± 1,000 yr B.P. (Table 1). The lack of major unconformities and paleosols in the older fan alluvium below or above this dated horizon implies that all of the exposed 13 m of the unit formed during the late Pleistocene epoch. Evidence discussed below supports a conclusion that the fan surface on the northeast side of the fault had become inactive by about 13,000 yr B.P.

FIGURE 2 EXPLANATION

UNITS

- Hl Low-channel alluvium
- Hh High-channel alluvium
- Hs Slope wash (mantles most of area, but mapped only where boundaries are d stinct)
- Py Younger-fan alluvium (dots indicate edges of individual lobes)
- Po Older-fan alluvium

SYMBOLS

- Contacts (solid where geomorphically apparent or exposed in trench, dotted where buried, dashed where inferred
- 0.3' Faults (as above; hachures on downthrown side; numbers indicate height of scarp)
- Selected small gullies offset ~9m in 1857
- 5 / 10 Trenches { backhoe / bulldozer
- Crests of small fans and source gullies offset ~9m in 1857
- 0.3' Landslide, showing headscarp, scarp height, and direction of movement

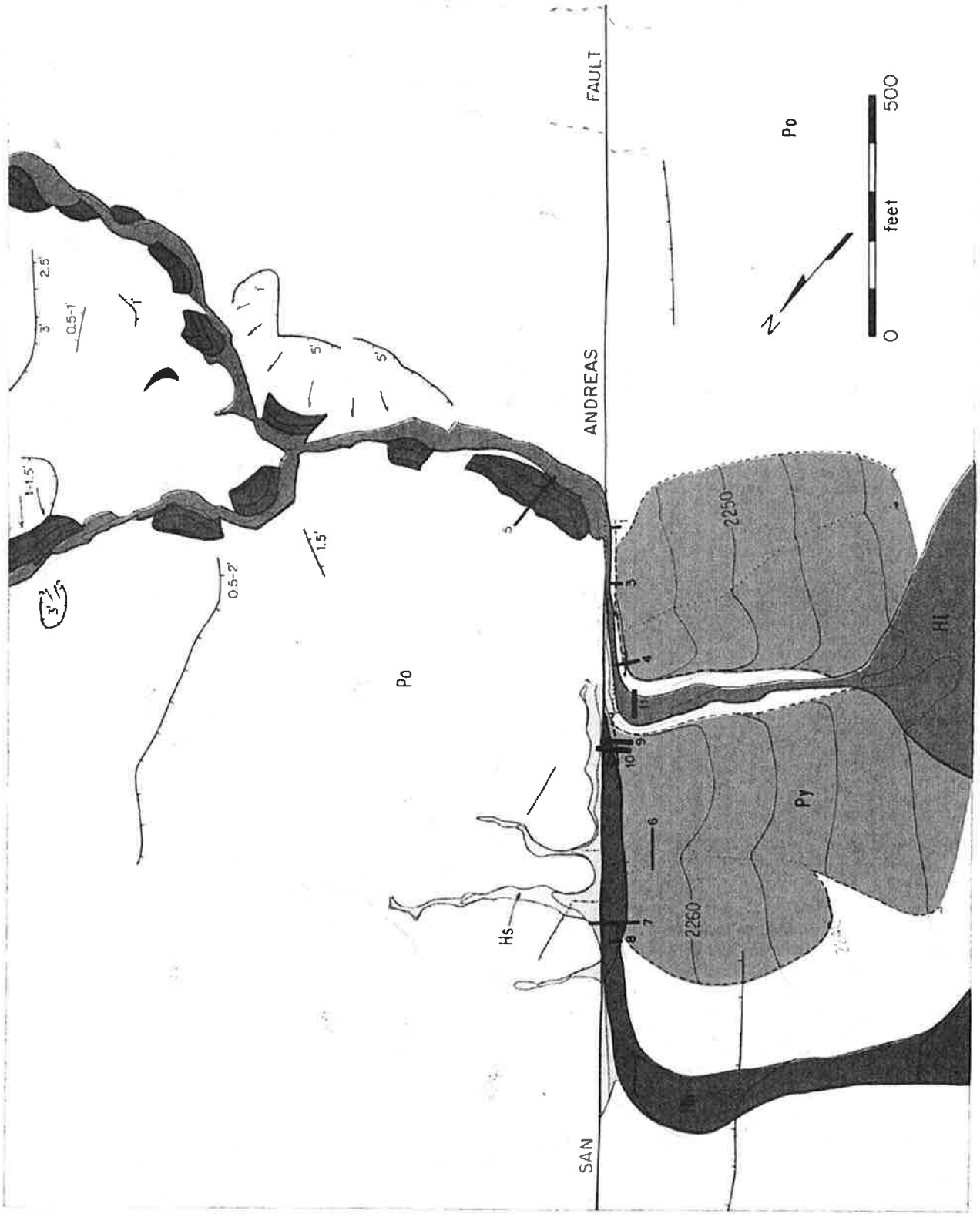

Figure 2. Geologic map of Wallace Creek. Contours of topographic base map show elevation (in feet) above sea level.

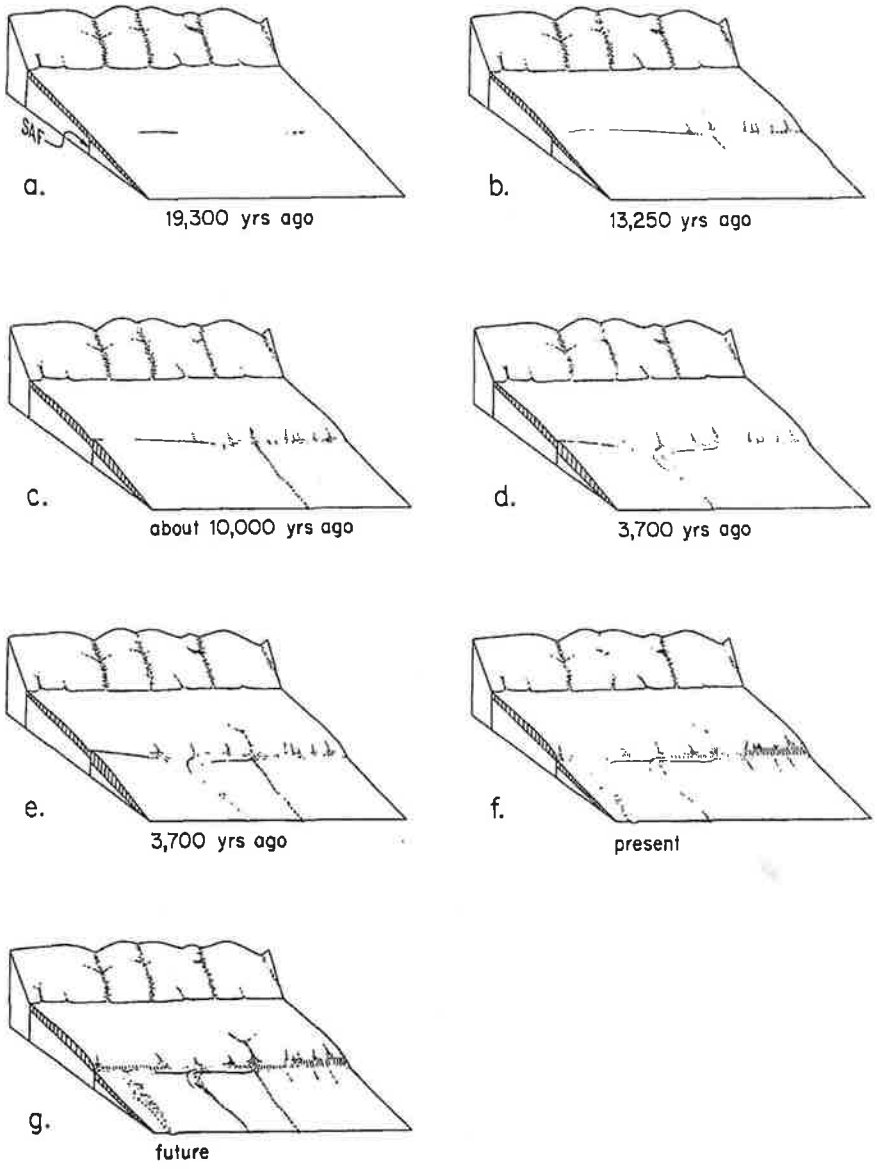

Figure 7. The Holocene–late Pleistocene evolution of Wallace Creek. An aggrading "older alluvial fan" during the period including 19,300 yr ago progressively buried small scarps formed along the San Andreas fault (SAF) during major strike-slip events (a). Right-lateral offsets accumulated during this period, but no geomorphologically recognizable offsets began to form until 13,250 yr ago, when the "older alluvial fan" became inactivated by initial entrenchment of Wallace Creek (b). At this time, erosion of small gullies to the right (southeast) of Wallace Creek also resulted in deposition of the "younger fan alluvium" downstream from the fault. These features then began to record right-lateral offset, and scarps began to grow along the fault. About 10,000 yr ago, a new channel was cut across the fault at Wallace Creek, and the initial channel, downstream from the fault, was abandoned (c). The new channel remained the active channel of Wallace Creek during the early and middle Holocene, during which ~250 m of slip accumulated (d). This channel filled with "high-channel alluvium" 3,700 yr ago, and Wallace Creek cut a new channel straight across the fault (e). Between 3,700 yr ago and the present, this youngest channel has registered 128 m of right-lateral offset (f). Aggradation of this channel, accompanied by continued offset, will probably lead to its abandonment and the creation of a new channel, cut straight across the fault (g).

intersection with the fault and then measuring the distance from that intersection to the intersection of the modern channel edge (labeled 2 in Fig. 8) with the fault. The same value is obtained if one measures the distance between the offset segments of the modern channel (labeled 3 and 4 in Fig. 8). In making the latter measurement of offset, it is important to realize that the outside edge of the left bend has been eroded by flood waters that have swept against it as they have passed around the left bend. The right bend has not been eroded in this manner, because it is refreshened each time the fault slips.

The fact that feature 1 and feature 3 (Fig. 8) intersect the fault at almost the same point strongly suggests that the abandonment of the high channel and entrenchment of the modern channel were contemporaneous. This coincidence also indicates that the new channel was cut straight across the fault without any initial nontectonic deflection of the stream along a fault scarp. The absence of any initial, nontectonic deflection is also confirmed by the fact that the modern channel is entrenched through a broad topographic high immediately downstream from the fault (consider contours in Fig. 2). If the channel had been deflected along a fault scarp, one would expect it to have cut through a low point on the downstream side of the fault rather than a high point. The measured separation of 128 m thus is ascribable entirely to tectonic offset.

The youngest date from the deposits of the abandoned high channel (3680 ± 155 yr B.P.) provides a maximum age for the modern channel, because all of the high-channel sediments were deposited before the modern channel was cut. All offset of the modern channel thus occurred between this date and A.D. 1857. The average slip rate, therefore, can be no slower than 35.7 ± 1.9 mm/yr [128 ± 1 m/3,680 ± 155 – 93 yr]. (93 yr is the time between A.D. 1950, which has been designated zero B.P., and A.D. 1857.)

Additional considerations are necessary to provide an upper limit to the slip rate. For this constraint, trenches 9 and 10 (Fig. 4) are useful. The high-channel deposits here consist of three distinct units, labeled C1, C2, and C3, that represent three distinct scourings and fillings. The uppermost sediment of channel C2 in trench 10 contained the radiocarbon sample the age of which is 3780 ± 155 yr B.P. At the time of deposition, C1, C2, and C3 in trenches 9 and 10 must have been at or northwest of the right bend of Wallace Creek. Trench 9 is now 145 m northwest of the right bend, and so no more than 145 m of dextral slip has accumulated since channel C2 was filled 3780 ± 155 yr B.P.

The trend of C2 between trenches 10 and 9 suggests that the edge of C2 actually intersects

slip rate represents the average rate of strain accumulation between large earthquakes. The recurrence intervals displayed in Table 2 may, therefore, be realistic estimates of the dormant intervals that preceded the past three great earthquakes.

In the next section, we attempt to assess when the current earthquake cycle will end at Wallace Creek; that is, when the next great earthquake, accompanied by rupture at Wallace Creek, will occur. We also attempt to use the 3,700-yr average slip rate to assess the likelihood of large earthquakes elsewhere along the San Andreas fault.

FORECASTS OF THE BEHAVIOR OF THE SAN ANDREAS FAULT

Along the South-Central (1857) Segment

If the crust adjacent to the San Andreas fault has been accumulating strain at 34 mm/yr since 1857, as much as 4.3 m of potential slip has now been stored and conceivably could be released along all or part of the 1857 rupture. Geomorphologic data, however, suggest that this is likely only along two portions of the 1857 rupture. Wallace Creek is not within either of these portions.

Figure 10 displays offsets measured along the south-central segment of the San Andreas fault. The 1857 segment is divisible into at least three parts, based on slippage during the 1857 earthquake and one to four previous large earthquakes. The southeastern part is ~90 km long and seems to have been characterized by 3- to 4.5-m slip events. The central 160 km, including Wallace Creek, has experienced 7 to 12.3 m of slip during the most recent 3 great earthquakes. The lower values along this central portion occur along the reach between km 90 and km 200, where several other active faults to the north and northeast exist, and so the lower values may reflect distributed deformation, away from the San Andreas fault. A 30-km segment northwest of Wallace Creek experienced 3 to 4 m of slip in 1857 and probably 1 or 2 during previous large earthquakes, as well.

These data suggest that each part of the fault has experienced a characteristic amount of slippage during the past three to four large earthquakes. Although, of course, so few data do not provide a statistically sound basis for predicting all previous and future events, we are confident that this pattern offers some insight into the long-term behavior of the fault.

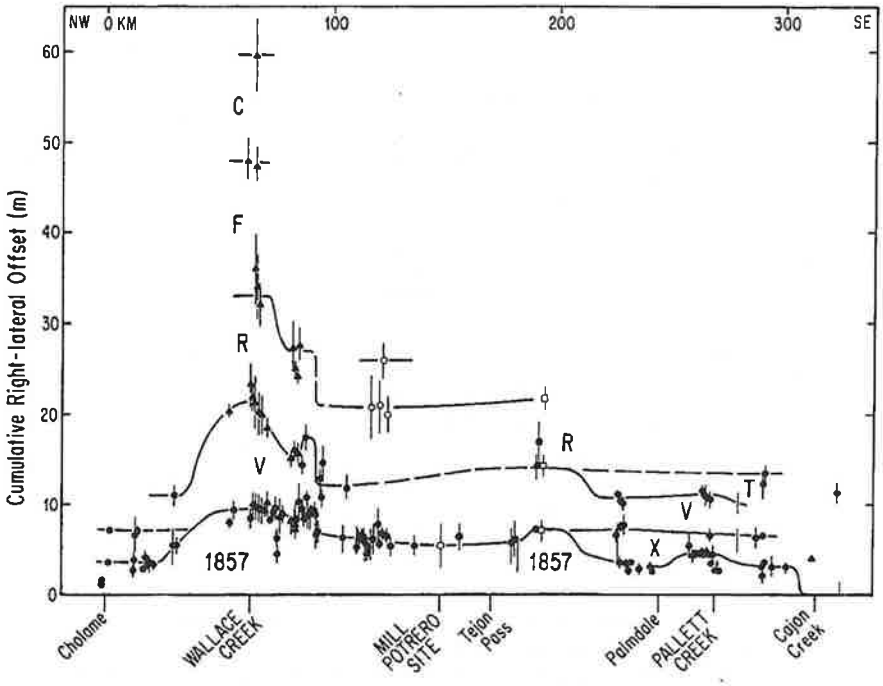

Figure 10. Right-lateral offsets measured along the south-central (1857) segment of the San Andreas fault suggest that slip at each locality is characterized by a particular value. Solid circles are data from Sieh (1978c), with poor-quality data deleted. Open circles are data from Davis (1983). Triangles are new data and remeasurements at sites reported by Sieh (1978c). Open squares are new data. Vertical bars indicate magnitude of imprecision in measurement.

At least two explanations are worth considering. First, we consider the possibility that the northwestern 40 km and southeastern 90 km are loaded more slowly, and, therefore, when the earthquake occurs, they experience lesser amounts of slip than does the central 160-km-long part. This is unlikely, because the average Holocene slip rate along these two parts must be nearly equal to the rate determined at Wallace Creek. Just beyond the south-central segment, at Cajon Creek (Fig. 10), the San Andreas has average Holocene and late Holocene slip rates of 25 ± 3 mm/yr (Weldon and Sieh, 1981). The nearby San Jacinto and related subparallel faults probably carry ~10 mm/yr at this latitude (based on data of Sharp, 1981, and Metzger, 1982). These fault systems end and nearly merge with the San Andreas fault just northwest of Cajon Creek. Farther northwest, the San Andreas fault is the only major active structure, and so northwest of Cajon Creek, it must have a slip rate of ~35 mm/yr. In addition, the average recurrence interval for large earthquakes at Pallett Creek (location in Fig. 10) is in the range of 145 to 200 yr, which is appreciably shorter than the 240- to 450-yr range at Wallace Creek. For this reason, some of the slip events shown in Figure 10 in the Palmdale–Pallett Creek region must have their northwestern rupture tip southeast of Wallace Creek, and 1857-like events cannot be the only type of slip event along this part of the south-central segment.

The northwestern 30 km of the south-central segment (Fig. 10) must also share the long-term average slip rate of Wallace Creek. No diversion of a large fraction of the Wallace Creek rate along other structures is plausible. The only known major active(?) fault nearby is the San Juan Hill fault, which runs 3 to 14 km west of and subparallel to the San Andreas from about Cholame to Wallace Creek (Jennings and others, 1975). Its rate of slip is probably no more than a few millimetres per year.

A second explanation for the different behavior of the three parts of the south-central segment is based on the hypothesis that each part is imbued with a different strength. If, for reasons of geometry or rock properties, the central 160 km of the segment were 2 or 3 times stronger than the 2 other parts, 2 or 3 times as much elastic loading of the adjacent crustal blocks would be necessary before failure occurred.

Each failure thus would result in two to three times as much slippage as on the two adjacent parts. Such an explanation is compatible with our judgments that (1) slip rate does not vary greatly along the south-central segment, and (2) large earthquakes are more frequent at Pallett Creek than at Wallace Creek.

Table 3 lists our best estimates of the dates of large earthquakes at Wallace Creek and proposed correlations with large earthquakes that have been directly dated at Pallett Creek (Sieh, in press) and at Mill Potrero (Davis, 1983). The capital letters in Figure 10 reflect our best judgment regarding correlation of the latest events at Wallace Creek, Pallett Creek, and Mill Potrero. Event X at Pallett Creek (A.D. 1720 ± 50) has no correlative at Wallace Creek, although Davis (1983) discovered evidence for and dated a relatively small slip event at Mill Potrero that may well be event X. Event V at Pallett Creek occurred about A.D. 1550, which is about the time we estimate that the last prehistoric event at Wallace Creek occurred, and also about the time of a large slip event that Davis (1983) discovered at Mill Potrero. Similarly, events R and F at Pallett Creek occurred at about the time we estimate that the third and fourth events occurred at Wallace Creek.

On the basis of the foregoing discussion, we judge that the central 160 km of the south-central segment of the San Andreas fault is unlikely to generate a great earthquake for at least another 100 yr. Recurrence intervals appear to be in the range of 250 to 450 yr, and yet the time elapsed since the great earthquake of 1857 is only 127 yr. Slip during the latest 3 great earthquakes has been 7 to 12.3 m, and yet we suspect that only a little more than 4 m of potential slip has been stored in the past 127 yr.

The southeastern 90 km and the northwestern 30 km of the south-central segment are good candidates for producing a large earthquake within the next several decades. Geomorphologic measurements seem to indicate that 3 to 4.5 m of slip is characteristic during large events, and >4 m of potential slip may well have been stored in the adjacent crustal blocks since 1857. Based on studies at Pallett Creek, the probability of a great event along the southeastern 90 km of the south-central segment within the next 50 yr is between 26% and 98% (Sieh, in press).

Along the Creeping Segment

The long-term average slip rates determined at Wallace Creek are indistinguishable from the geodetically determined rates of slip at deep levels along the fault from Wallace Creek to Monterey Bay (Savage, 1983; Lisowski and Prescott, 1981). The long-term rates at Wallace Creek are also identical to the historical rate of slip at shallow levels along the central 50 km of the creeping segment (see data compiled by Lisowski and Prescott, 1981, Fig. 6). These similarities could be coincidental, but they suggest that the central 50 km of the creeping segment is creeping annually at its millennial-average rate of slip. If this were true, it would mean that large elastic strains are not accumulating across the central 50 km of the creeping segment, and that this segment will not participate in the generation of the next large earthquakes along the San Andreas fault.

From a geological point of view, it is reasonable to suspect that the long-term slip rate along the San Andreas fault at Wallace Creek should not be different from its long-term rate along the creeping segment, except along its northernmost 50 km, adjacent to which runs the actively creeping Paicines fault (Harsh and Pavoni, 1978). No other large, active structures in the latitudes of the creeping segment can be called upon to absorb a large portion of the slip rate observed farther south at Wallace Creek. Likewise, there are no obvious geological structures near the San Andreas that would lead one to suspect that the long-term slip rate along the creeping segment is appreciably higher than the long-term rate farther south.

Along the 90-km Segment Centered on Cholame

Between the central 50 km of the creeping zone and Wallace Creek, there is a stretch of the San Andreas fault that historically has been a zone of transition between the fully creeping and fully locked portions of the fault. On the basis of available data, this segment is a prime candidate for generating a large earthquake in the near future. In the period of historical record, it has not experienced as much slip as have segments to the northwest or southeast, and it is therefore a "slip gap."

One interpretation of the historical data is illustrated in Figure 11, in which cumulative right-lateral slip for the past two centuries is

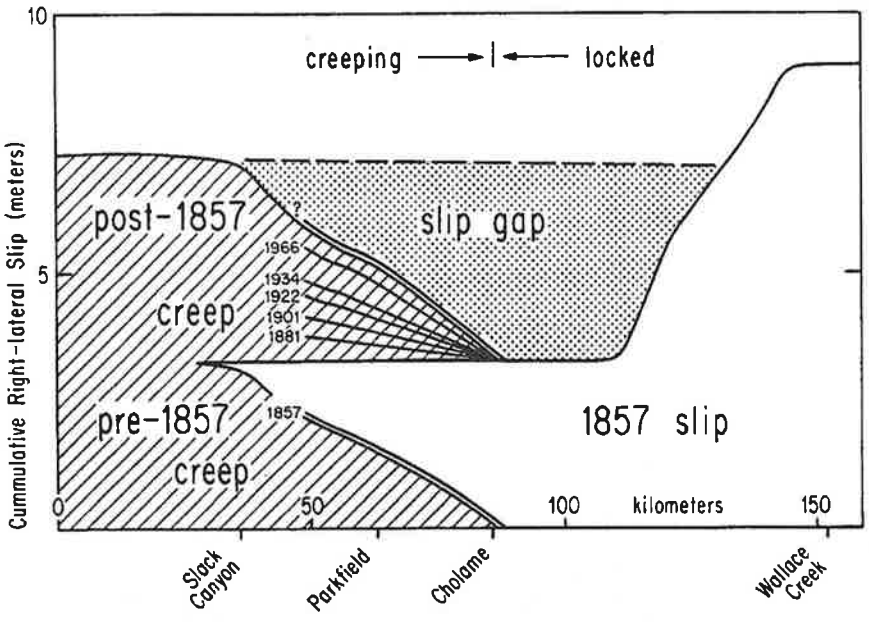

Figure 11. Hypothetical source of future major earthquake along the San Andreas fault includes ~60 km of the currently creeping segment and 30 km of the locked segment. Cumulative right-lateral slip plotted against distance along the fault indicates that this 90-km segment is slip-deficient relative to adjacent stretches of the fault. Slip in 1857 is from Sieh (1978c). Cumulative slip along the creeping segment is extrapolated from alignment array slip rates for period 1968–1979 (Lisowski and Prescott, 1981, Fig. 6). Dates of moderate earthquakes generated by slip along the fault in the Parkfield-Cholame region are shown, because such an event probably triggered the great 1857 rupture and conceivably could trigger the rupture of the slip gap.

Six similar sequential ruptures of the San Andreas fault, Carrizo Plain, California

Jing Liu
Yann Klinger
Division of Geological and Planetary Sciences, California Institute of Technology, Pasadena, California 91125, USA, and
Laboratoire de Tectonique, Institut de Physique du Globe de Paris, 4 place Jussieu, 75252 Paris cedex 05, France
Kerry Sieh*
Division of Geological and Planetary Sciences, California Institute of Technology, Pasadena, California 91125, USA
Charles Rubin
Department of Geological Sciences, Central Washington University, Ellensburg, Washington 98926, USA

ABSTRACT

We document the precise sizes, but not the dates, of the six latest offsets across the San Andreas fault at Wallace Creek, California. Three and perhaps four of these, including the latest in 1857, show dextral offset of 7.5–8 m. The third and fourth offsets, however, are just 1.4 and 5.2 m. The predominance of similar offsets for the latest six events suggests that the fundamental properties of the fault system that control slip size do not vary greatly from event to event. The large offsets imply that ruptures involving this site are typically more than 200 km long.

Keywords: San Andreas, fault, paleoseismology, earthquake, rupture.

INTRODUCTION

Concepts and models of repeating fault rupture are tenuous, because there are few data to test them. Some advocate sequences that are highly regular in time or rupture parameters (e.g., Reid, 1910; Tse and Rice, 1986; Schwartz and Coppersmith, 1984; Lapusta et al., 2000). Others predict irregular behavior, where rupture parameters and frequency range over orders of magnitude (e.g., Bak and Teng, 1989; Carlson and Langer, 1989; Ben-Zion, 1996; Shaw and Rice, 2000). Probabilistic earthquake forecasts usually assume nearly periodic identical ruptures (e.g., Working Group on California Earthquake Probabilities, 2002), although combinations with other behaviors have also been attempted (e.g., Frankel et al., 1996; Giardini, 1999).

Acquiring data that constrain physical models is difficult, because repose times between large ruptures of a single fault are hundreds to thousands of years, far longer than observational histories. Paleoseismic methods, however, can produce records of fault slip through numerous earthquake cycles (McCalpin, 1996; Yeats et al., 1997). Some paleoseismic data show that slip at a given location is similar from one earthquake to the next (Sieh, 1996; Klinger et al., 2003; Streig et al., 2004). However, well-constrained paleoseismic data sets rarely contain more than two sequential ruptures. Longer records are usually based on indirect evidence or have large uncertainties in slip sizes (e.g., Schwartz and Coppersmith, 1984; Sieh, 1984; Pantosti et al., 1996).

Better long records would narrow the wide range of predicted behaviors. Thus our goal in this study was to document precisely many sequential offsets from a single fault site. We were half successful; we recovered a precise record of offsets for six sequential ruptures, but we could not determine precisely their dates.

DESCRIPTION OF THE SITE AND METHODS

The San Andreas fault in the Carrizo Plain is unusually simple and well expressed. Wallace (1968) first used small offset gullies here to estimate slip of the great 1857 and earlier earthquakes. Later work (Sieh, 1978) suggested that the latest three ruptures just southeast of Wallace Creek (Fig. 1A) were 9.5–12.5 m. Excavations by Grant and Sieh (1993) nearby yielded an 1857 offset of ~7 m. At Wallace Creek, Sieh and Jahns (1984) determined a late Holocene slip rate of ~34 mm/yr and speculated that at this rate, offsets of ~10 m would recur every ~300 yr.

At our Wallace Creek paleoseismic site (Fig. 1A), gullies downstream from the fault are dextrally offset from a solitary upstream channel (Fig. 1B). The shape of the youngest gully suggests ~7–10 m of slip in 1857 (Sieh, 1978; Grant and Sieh, 1993). Older offset gullies, farther northwest, are more subdued but still visible. Slope wash from the scarp partially buries these, so their precise geometry near the fault is obscure.

To determine exactly the number, size, and sequence of the dextral offsets, we exposed the subsurface shape and stratigraphy of the channels (Liu, 2003). We began by hand-digging narrow trenches across the gullies, 4–5 m from and parallel to the fault. After precisely surveying and mapping these trench walls, we cut into the wall closer to the fault in increments of 20 to 60 cm, progressively mapping each new exposure. In this manner, we carefully followed each potential piercing line into the fault zone. These three-dimensional excavations enabled us to reconstruct channel and fault geometries with errors of just a few centimeters.

EVIDENCE FOR BURIED OFFSETS

The excavations revealed 12 buried channels on the downstream side of the fault, beneath the four topographically obvious channels (Fig. 2A). Most of these were solitary channels with repeated scours and fills. The deeper parts of a channel commonly had sharp walls, made clear by the contrast of internal and external strata. Beds within a channel were commonly loose, pebbly, fluvial sand and colluvial debris, whereas strata cut by a channel typically were harder, massive, poorly sorted gravelly sand and silt. Channel fills were generally looser and darker than material outside the channels. Except for channels c, h, and j, the downstream channels intersect the

*Corresponding author. E-mail: sieh@gps.caltech.edu.

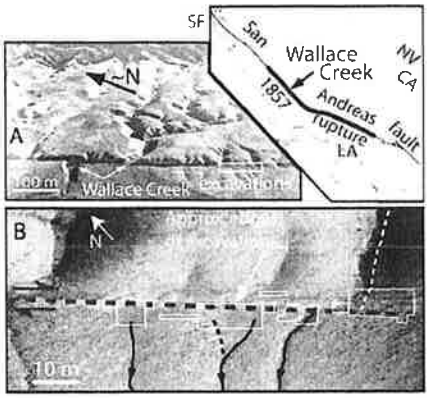

Figure 1. Two oblique aerial views of paleoseismic site. A: Small drainages few hundred of meters southeast of Wallace Creek offer unusual opportunity to determine offset size during past ruptures. Photo by P. Tapponnier. B: Four channels downstream from fault appear to be offset from single upstream channel.

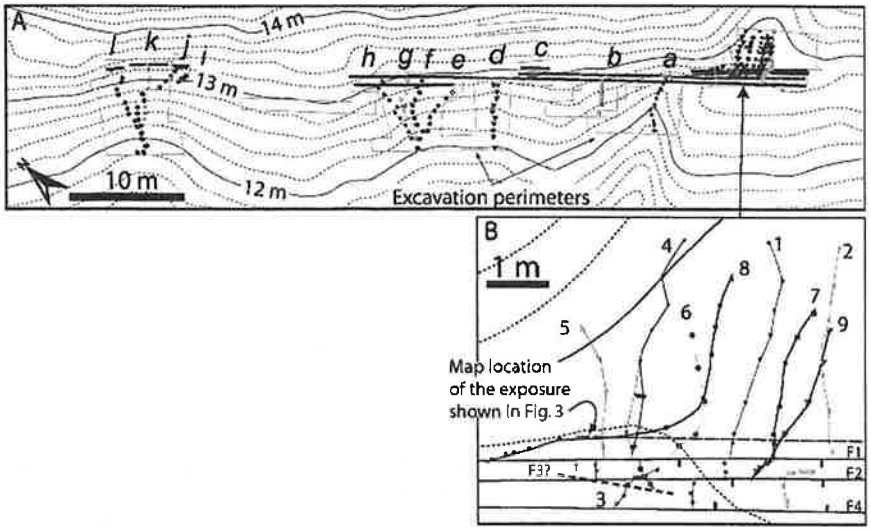

Figure 2. Map views of buried channels at site. Each colored symbol represents position of channel thalweg mapped and surveyed in excavation wall. Letters denote downstream channels and numbers represent upstream channels. Colors indicate correlations across fault. Gray and black lines are channels with no known correlatives across fault. Thick black lines indicate surface projections of fault traces. Ticks on faults F1, F2 and F4 show downthrown side.

fault at high angles. Channels e and i do not intersect the fault.

Upstream exposures revealed nine nested channels (Fig. 3). Several channels contain distinctive laminated beds of well-sorted fines, deposited as suspended load from water ponded behind shutter ridges after large offsets. Most of these channels intersect the fault at a high angle (Fig. 2B). The internal stratigraphy and shape of both upstream and downstream channel segments constrain fault rupture and warping to a narrow zone (Fig. 2). Distortion in channel shape and warping of channels due to shearing appear only within tens of centimeters of the fault traces.

We can match the youngest five channel pairs across the fault (Fig. 4). Correlation of the sixth pair is less certain. Matches are based on (1) crosscutting relationships in the upstream exposures, (2) shapes and internal stratigraphy of the channels, and (3) angles at which channels intersect the fault. Radiocarbon analyses of detrital charcoal show that all six matched channels formed in the past ~1 k.y., and that all the uncorrelated channels are at least 2500 yr old (Liu, 2003). Ranges of ages within individual channels are as great as 1 k.y., however, so it is clear that significant reworking of carbon has occurred. Thus, individual channel ages are poorly constrained.

Crosscutting relations of clustered channels (e.g., e, f, g, and h) allow determination of relative ages of some downstream channels. The relative ages of most of the upstream channels are clear from their crosscutting relations (Fig. 3). However, some of these relations have been obliterated by erosion. For example, the stratigraphic relation of channel 2 to channels 4, 5, and 6 is uncertain, due to incision of younger channel 1. Fortunately, matching of channel shapes and internal stratigraphy with channels across the fault zone resolves such ambiguities in relative age. Thus, the evidence is strong for the correlation of upstream channels 1, 2, 3, 4, and 5 with downstream channels a, b, c, d, and g, respectively. The match of channels 6 and h is less certain, because younger channels have eroded much of channel 6. The correlation of 6 and h is based upon channel size, fill, and the acute angle of intersection of both channels with the fault. Channel 6 is the only upstream channel to trend southward near the main fault, and so its downstream equivalent should also trend southward away from the fault.

Upstream channels 7, 8, and 9 and downstream channels e, f, i, j, k, and l have no correlatives within the excavated volumes. Downstream correlatives of channels 7, 8, and 9 likely exist farther to the northwest, and upstream correlatives of channels e, f, i, j, k, and l probably reside farther southeast. Sparse radiocarbon ages of ≥2500 yr on detrital charcoal within these older channels support this inference (Liu, 2003).

OFFSET SEQUENCE

Matching thalwegs and other channel features across the fault allows us to recover their horizontal and vertical offsets, because we can

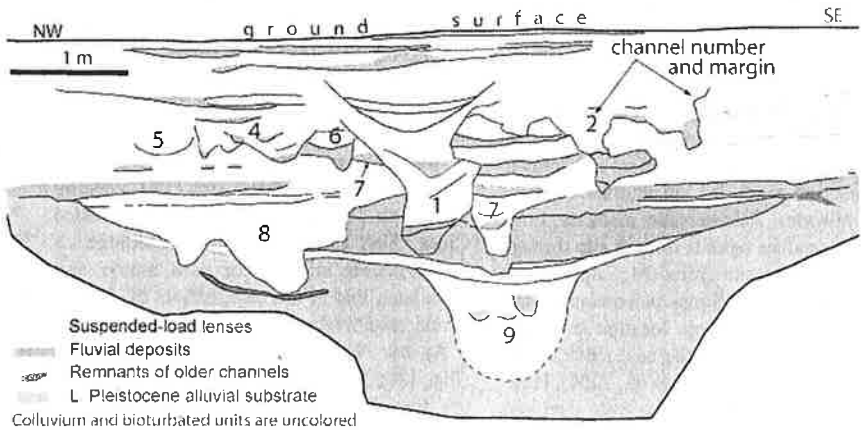

Figure 3. Simplified map of wall of upstream excavation shows eight of nine nested channels. Suspended-load deposits attest to temporary ponding behind shutter ridges after large dextral offsets. Channel 3 does not extend upstream as far as cross section. Many channel strata have been bioturbated, but enough fluvial stratigraphy remains, especially in lower portions of channels, to enable correlation of units across fault.

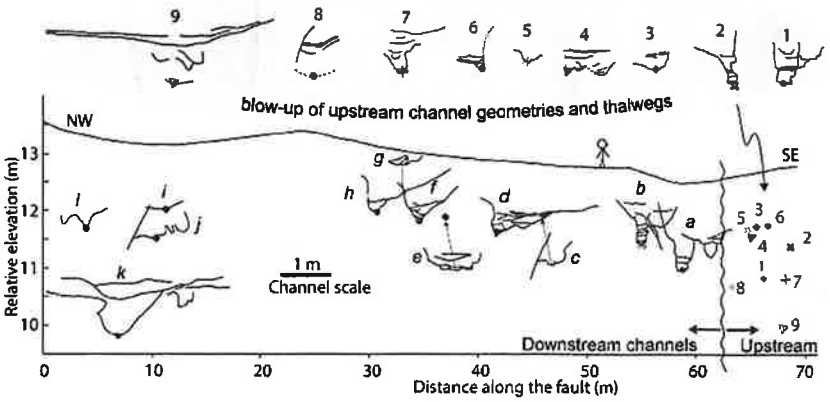

Figure 4. Relative locations of downstream and upstream channel bottoms (thalwegs) at their intersection with fault, projected onto vertical plane parallel to fault. Wavy vertical line separates domains of upstream and downstream channels. Downstream channel shapes and strata appear at enlarged scale atop their thalwegs. Thalwegs of upstream channels are nested close together, so details of their shapes and strata appear within shaded ellipse above vertical section. Figure 3 shows stratigraphic relations of these upstream channels. Colors show correlative upstream and downstream thalwegs.

reconstruct channel geometries in three dimensions (Fig. 5). For example, the size of event WC1 (7.9 ± 0.1 m) is the dextral offset of channel pair 1 and a. The vertical offset is only a few centimeters, southwest side up. The size of penultimate event WC2 (7.6 ± 0.4 m) is the offset of channel pair 2 and b minus the offset of pair 1 and a. The vertical offset is ~10–15 cm, northeast side up. Offset WC6 is the only equivocal one. The acuteness of the intersection angles allows that the offset could be substantially >5.4 ± 0.6 m.

Altogether, ~36 m of dextral slip has accumulated in six discrete episodes. The size of the offsets, from oldest (WC6) to youngest (WC1), is ≥5.4, 8.0, 1.4, 5.2, 7.6, and 7.9 m (Fig. 5). Uncertainty is commonly a few tens of centimeters or less, because of the precision of the surveying and the sharpness of the stratigraphic piercing points. Cumulative vertical offset is nil, although for individual offsets the vertical component ranges as high as ~30 cm.

None of these six youngest offsets likely represents more than one rupture event. Frequent alluvial cuts and fills have resulted in two or more subordinate cuts and fills within each of the channels. We would expect deflections of subordinate cuts and fills near the fault if offset had occurred soon after their formation. The lack of such deflections suggests that the offsets represent single events.

The gully occupied by channel pairs 4 and d and 3 and c underwent a clear postoffset deflection (Liu, 2003). The deeper, older parts of the gully are segments 4 and d (Fig. 2A). These segments intersect the fault at nearly right angles and thus appear to have been normal to the fault prior to offset. Channel c, higher in the fill sequence, trends southeastward near the fault. Another piece of channel c appears within the fault zone still farther southeast, extending at a very acute angle to the fault zone. Its correlative is upstream channel 3, which strikes at an acute angle to the fault trace and does not continue far upstream. The relations of channel pairs 4 and d and 3 and c thus demonstrate that a channel was offset ~1.4 m, then reoccupied by a new, deflected channel, which was later offset an additional 5.2 m (Liu, 2003). This example of subtleties in site stratigraphy suggests that if any of the other discrete offsets represented more than one event, each would be recognizable in the internal stratigraphy of the channels.

Furthermore, the abrupt termination of channel walls and channel stratigraphy at the fault strongly suggests that the offsets occurred suddenly. The lack of dog-leg deflections in channel stratigraphy (other than in the case of channel pair 3 and c) and the narrowness of the channels support our analysis that the latest 36 m of dextral offset have accumulated in just six sudden events (Liu, 2003). The channel shapes and their infills might not allow discrimination of events that occurred just a few days or months apart.

IMPLICATIONS

The Wallace Creek paleoseismic site has yielded a long and precise, albeit poorly dated, sequence of serial fault ruptures. Three and possibly four of the six offsets are between 7.5 and 8 m, and ~95% of recent slip has accrued in 5.2–8.0 m increments. This means that slip sizes are much closer to regular than to stochastic (Liu, 2003), and that those properties of the fault system that control slip size vary little from event to event. Furthermore, the accrual of offset predominantly in increments of 5.2–8 m supports the concept of the earthquake cycle, wherein strain is slowly stored and then quickly released during large, similar dislocations (Reid, 1910; Tse and Rice, 1986; Lapusta et al., 2000).

Our data do not support models that produce great complexity of fault slip, including those that generate power-law frequency-size distributions of seismicity on single faults (e.g., Shaw and Rice, 2000). Such models predict variability in offset values over orders of magnitude. Physical models that produce more uniform rupture sequences, with populations of slip sizes like those seen at our site, use smoothing parameters and assume rupture patches with uniform frictional properties along strike, large critical-patch size for rupture preparation, or a high degree of geometrical or material regularity within fault zones

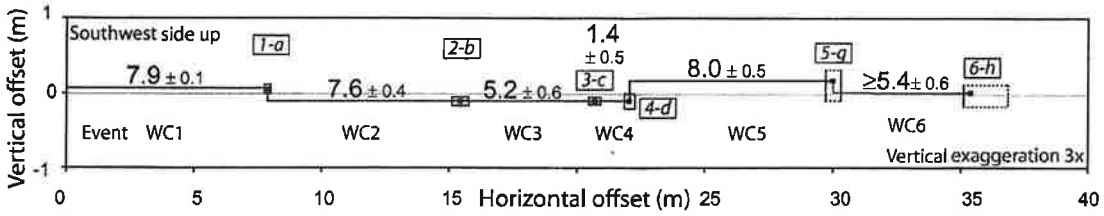

Figure 5. Horizontal and vertical offsets of channel pairs derived from data in Figure 4. Letter-number pairs in boxes are correlated channels. Uncertainties in horizontal and vertical offset of each pair appear as small black rectangle (Liu, 2003). Amount of dextral offset for six discrete ruptures (WC1–WC6) ranges from 1.4 to 8.0 m, but at least three and perhaps four are between 7.5 and 8.0 m. Vertical components of slip are small fractions of dextral offset, and their sense varies through sequence.

JOURNAL OF GEOPHYSICAL RESEARCH, VOL. 114, B01313, doi:10.1029/2007JB005285, 2009

Revised dates of large earthquakes along the Carrizo section of the San Andreas Fault, California, since A.D. 1310 ± 30

Sinan O. Akciz,[1] Lisa Grant Ludwig,[1,2] and J Ramon Arrowsmith[3]

Received 20 July 2007; revised 15 September 2008; accepted 29 October 2008; published 27 January 2009.

[1] Precise knowledge of the age and magnitude of past earthquakes is essential for characterizing models of earthquake recurrence and key to forecasting future earthquakes. We present 28 new radiocarbon analyses that refine the chronology of the last five earthquakes at the Bidart Fan site along the Carrizo section of the south central San Andreas Fault, which last ruptured during the Fort Tejon earthquake in A.D. 1857. The new data show that the penultimate earthquake in the Carrizo Plain occurred not earlier than A.D. 1640 and the modeled 95th percentile ranges of the three earlier earthquakes (and their mean) are A.D. 1540–1630 (1585), A.D. 1360–1425 (1393), and A.D. 1280–1340 (1310), indicating an average time interval of 137 ± 44 years between large earthquakes since A.D. 1310 ± 30. A robust earthquake recurrence model of the Carrizo section will require even more well-dated earthquakes for thorough characterization. However, these new data imply that since A.D. 1310 ± 30, the Carrizo section has failed more regularly and more often than previously thought.

Citation: Akciz, S. O., L. Grant Ludwig, and J R. Arrowsmith (2009), Revised dates of large earthquakes along the Carrizo section of the San Andreas Fault, California, since A.D. 1310 ± 30, *J. Geophys. Res.*, *114*, B01313, doi:10.1029/2007JB005285.

1. Introduction

[2] The biggest challenge in understanding the long-term rupture behavior of an active plate-bounding fault, like the San Andreas Fault (SAF), and forecasting future large earthquakes along it is the paucity of long records of paleoseismic data, and in particular, accurate determination of the temporal distribution of past earthquakes. Along the southern SAF, there are only two paleoseismic sites where more than ten large surface rupturing earthquakes are thoroughly documented and well dated: Pallett Creek [*Sieh*, 1978, 1984; *Sieh et al.*, 1989] and Wrightwood [*Fumal et al.*, 1993, 2002; *Scharer et al.*, 2007; *Weldon et al.*, 2002] (Figure 1). Other sites along the southern SAF (Figure 1) exist, but the number of documented earthquakes and their age constraints are inadequate to represent the faulting behavior of the southern SAF.

[3] The Carrizo section of the southern SAF, where the Bidart Fan site is located, last ruptured on January 9, 1857 during the great Fort Tejon earthquake [*Sieh*, 1978] (Figure 1). Early earthquake geology research conducted near the Wallace Creek site in the Carrizo Plain supported the widely held view that this section of the SAF ruptures relatively infrequently (250–450 years) and only in large earthquakes with centuries long recurrence times [*Sieh and Jahns*, 1984] (Figure 1). A subsequent paleoseismological study at the Bidart Fan site [*Grant and Sieh*, 1994] (hereinafter referred to as GS94) reported ages of the five most recent earthquakes on the basis of interpretation of three paleoseismological excavations and a total of 14 radiocarbon analyses. Data presented by GS94 indicated a long interval of 350 to 450 years between 1857 and the penultimate earthquake (A.D. 1405–1510), and shorter intervals (~100 years) between the prior three large earthquakes on the Carrizo section. These limited data suggested temporal clustering since the early A.D. 1200s, a behavior similar to that first reported for the SAF at Pallett Creek [*Sieh et al.*, 1989]. The number of dated earthquakes was, however, too small to determine whether the Carrizo section is currently within a cluster of earthquakes with high probability of near-term rupture, or between clusters with relatively low probability of rupture. The *Working Group on California Earthquake Probabilities* (*WGCEP*) [1995] assumed that future earthquakes along the Carrizo section would be like the 1857 rupture and adopted a mean recurrence interval of 206 years, by using an estimated "characteristic displacement" value of 7±4 m [*Grant and Donnellan*, 1994; *Grant and Sieh*, 1993, 1994; *Sieh and Jahns*, 1984] and a late Holocene slip rate of 34 ± 3 mm/a [*Sieh and Jahns*, 1984].

[4] There are two main reasons why earlier studies in the Carrizo Plain (and elsewhere) led to large uncertainties in the dates of paleoearthquakes. First, paleoseismological investigations conducted in the 1970s through early 1990s had to rely on a limited number of radiocarbon ages, as many of the collected samples were too small to be dated at the time. Recent advances in radiocarbon dating by accelerator mass spectrometry (AMS) permit routine dating of much smaller samples than in the past. Now paleoseismologists can derive

[1]Program in Public Health, University of California, Irvine, California, USA.
[2]California Institute for Hazards Research, University of California, Irvine, California, USA.
[3]School of Earth and Space Exploration, Arizona State University, Tempe, Arizona, USA.

0148-0227/09/2007JB005285$09.00

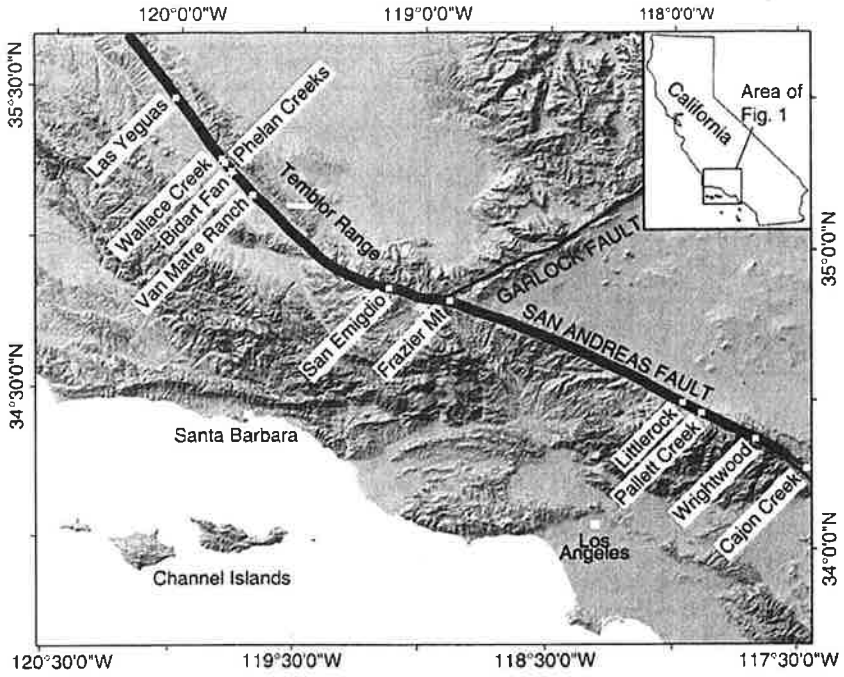

Figure 1. Location of the Bidart Fan site (marked with white star) with respect to other paleoseismic sites (white squares) along the southern San Andreas Fault zone. The Garlock Fault and the southern extent of the 1857 Fort Tejon earthquake rupture (heavy line) are also shown.

more accurate earthquake ages by analyzing samples from stratigraphic units that were never dated before and/or analyzing additional samples from units whose ages were constrained by only a single date. The second improvement is that the variance of initial age distributions for a stratigraphic unit or an earthquake obtained via the ^{14}C calibration may now be reduced by the application of Bayes' theorem if additional radiocarbon age data from underlying and overlying strata are available. Several different statistical computer programs, such as OxCal [*Ramsey*, 2005] and BCal (C. E. Buck et al., BCal: An online Bayesian radiocarbon calibration tool, 2001, available at http://bcal.sheffield.ac.uk), which were originally developed for archeologists, are readily available and applicable to paleoseismology problems [e.g., *Lienkaemper et al.*, 2002; *Young et al.*, 2002; *Dawson et al.*, 2003]. Other programs were specifically developed for paleoseismologists to estimate stratigraphic layer and earthquake ages [e.g., *Biasi et al.*, 2002; *Hilley and Young*, 2008].

[5] In this study, we dated 28 archived samples from the Bidart Fan site of GS94 to better constrain the age of the last five earthquakes that ruptured the Carrizo section of the SAF. We chose the Bidart Fan site for two main reasons.

[6] 1. Historically, paleoseismologic data from the Carrizo section of the SAF have been influential in the way the southern SAF behavior is interpreted [e.g., *Sieh and Jahns*, 1984; *Grant and Sieh*, 1994; *Liu et al.*, 2004; *Liu-Zeng et al.*, 2006; *Noriega et al.*, 2006; *WGCEP*, 1988, 1995, 2008] and the paleoseismological investigations at the Bidart Fan site has produced the only peer-reviewed and published earthquake age constraints [*Grant and Sieh*, 1994]. Therefore, it is important to better constrain the ages of the paleoearthquakes at the Bidart Fan site or at least verify the existing constraints to improve or confirm our current understanding of the behavior of this section of the SAF.

[7] 2. Organic samples including in situ burned grass fragments, charred twigs, and unidentified charcoal pieces from the Bidart Fan site collected and archived by *Grant* [1993], as a part of her dissertation, were readily available to conduct this investigation.

[8] In the following sections, we briefly describe our sampling methodology. We then summarize the earthquake evidence found in each of the three trench exposures. The evidence is discussed in detail by *Grant* [1993] and GS94. When following unit labels, earthquake descriptions, and sample locations, we refer readers to redrafted versions of *Grant*'s [1993] original trench logs published here completely in digital format as auxiliary material Figures S1, S2, and S3.[1] Note that this makes the complete logs available to a broader audience, given that GS94 only published critical portions of the logs for brevity. Important portions of the logs are included in Figures 5 and 7. We also include a table containing a systematic evaluation of the quantity and the quality of paleoearthquake evidences (following the method described by *Scharer et al.* [2007] and discussed in Tables 1–3). Finally, we describe how we obtain the new age constraints on the last five earthquakes at the Bidart Fan site and discuss their implications.

2. Chronological Methods

[9] In the work of GS94, a total of two samples were used to constrain the ages of both the penultimate (event B) and

[1] Auxiliary materials are available in the HTML. doi:10.1029/2007JB005285.

35

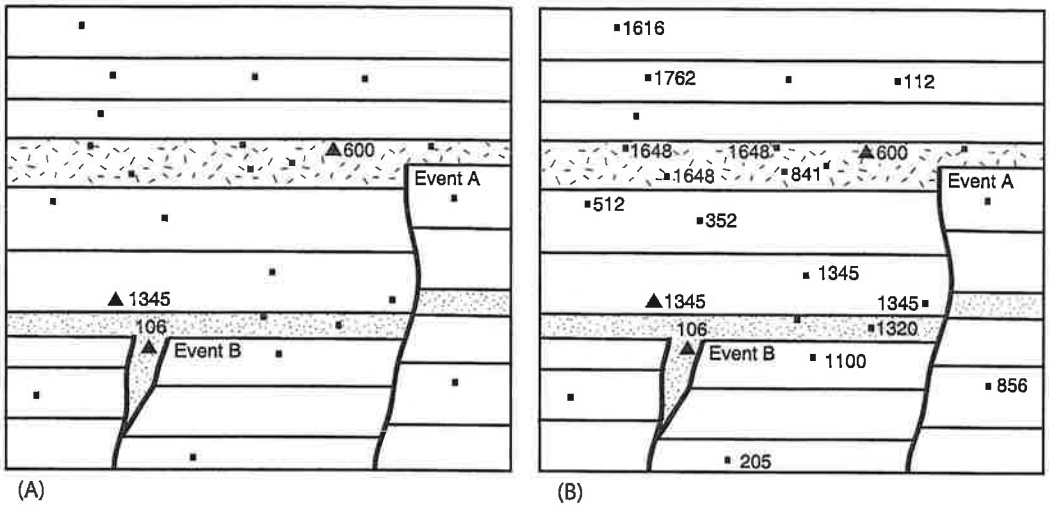

Figure 2. Illustrations of how additional age constraints from an entire stratigraphic section exposed in a trench wall can significantly improve the earthquake age estimates. The hypothetical trench log shows the preserved evidence for two paleoearthquakes and locations of detrital organic samples that were collected. Black triangles represent large organic samples, while black squares represent small ones. Numbers by the sample locations, which are also hypothetical, indicate the mean value of the calibrated radiocarbon ages in A.D. (a) In the case where there is a limitation on the size of the organic sample that could be dated, earthquake age determinations might be poor. Note the stratigraphic inversion that results from the lag between the initiation of the ^{14}C clock (e.g., a burn) and the deposition: 600 is above 1345. The data in this example indicate that event B occurred sometime before A.D. 1345 while event A occurred sometime after this date. (b) In the case where additional samples can be dated, event chronologies are significantly improved. Reworked samples from older sediments and samples from burned originally older wood are easier to identify. The data now indicate that event B occurred sometime between A.D. 1100 and A.D. 1320 and event A occurred sometime between A.D. 1345 and A.D. 1648.

Upon discussion with L. B. Grant, who originally hand-picked BDT2-22 fragments for analyses, we concluded that it is possible that BDT2-22 age (from GS94) represented the age of a mixture of grass and twig or some other wood flakes.

[18] The plot of the Bayesian model which constrains the timing of paleoearthquakes preserved at BDT2 is shown in Figure 6b. In addition to samples BDT2-10 and BDT2-35, we have also excluded samples BDT2-7 and BDT2-22 as they fell below the OxCal suggested 60% agreement index

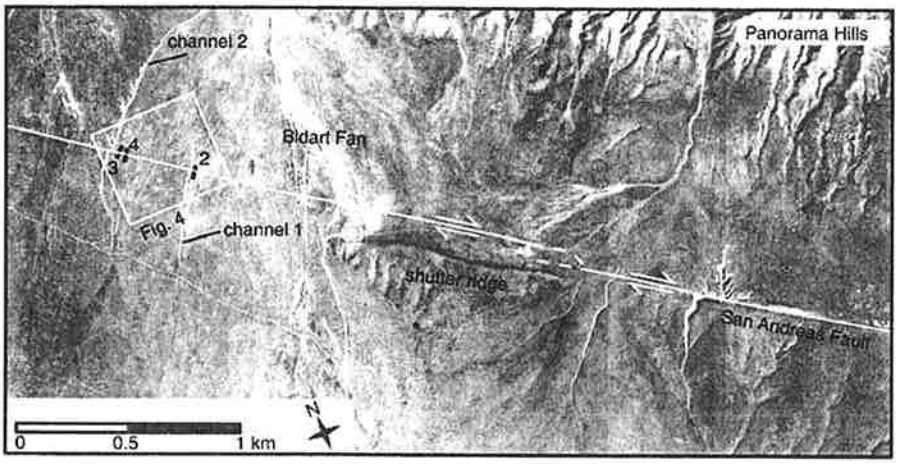

Figure 3. A 1932 aerial photograph (from the Fairchild Aerial Photography Collection) showing the 1857 (and earlier) rupture traces at the Bidart Fan. Labeled trench locations (2, BDT2; 3, BDT3; and 4, BDT4) are from *Grant and Sieh* [1994].

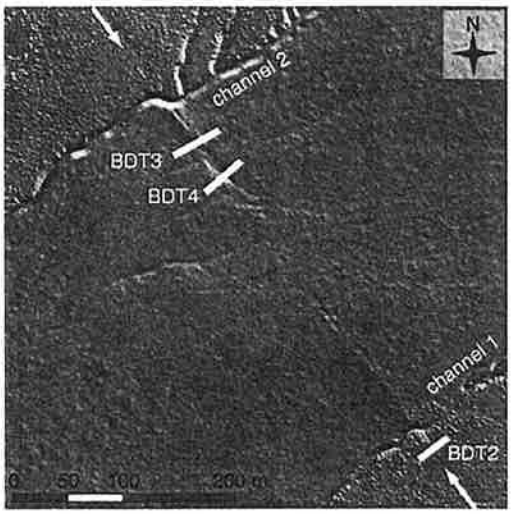

Figure 4. Trench locations of *Grant and Sieh* [1994] with respect to two right-laterally offset ephemeral channels (channels 1 and 2) are shown on a 25 cm resolution spline-derived DEM from B4 data set (http://www.earthscience-s.osu.edu/b4). Trace of the San Andreas Fault, located between the two black arrows, is partially buried by post-1857 sedimentation, though the active lobe of the fan is currently farther to the SE.

threshold during its MCMC simulation. We also interpreted the age of BDT2-25 from the paleosol section of unit 8 to represent the age of the paleosol and not necessarily the age of BDT2-b, as we agree with *Hilley and Young* [2008] that the GS94 use of paleosol formation as an absolute dating tool is currently unjustified even though the paleosol defines the event horizon. The new model age range for event BDT2-b is A.D. 1540–1630 (Figure 6b). This age is considerably younger than the age range preferred and reported by GS94 (A.D. 1405–1510).

3.2. BDT4

[19] In trench BDT4, the most recent earthquake (BDT4-a) that ruptured unit 40 is the A.D. 1857 earthquake (see Figure 7, auxiliary material Figure S3, and Table 4). Unit 50 was at the ground surface when event BDT4-b occurred. The stratigraphic unit which constrains the age of BDT4-b is unit 50. Of the three samples from unit 50 that we picked under the microscope (BDT4-51, BDT4-59, and BDT4-91), we were able to date one detrital charcoal fragment (BDT4-51) which yielded a calendar date of A.D. 1620–1960 (Table 4). This indicates that event BDT4-b occurred after A.D. 1620. Lack of datable material from units above BDT4-b prevents us from constraining the upper bounding age other than A.D. 1857, the date of the most recent earthquake.

[20] Direct evidence for earthquake BDT4-c is sparse and not high quality, as listed in Tables 1–3. The evidence can be interpreted in a couple of different ways: (1) BDT4-c was a small magnitude earthquake and caused minimal surface deformation at BDT4, or (2) some of the wide fault zones seen in BDT4 walls actually ruptured during BDT4-c, but the A.D. 1857 and/or the penultimate earthquakes ruptured these zones and disrupted evidence. We agree with GS94 interpretation of earthquake BDT4-c rupturing up to the top of unit 70 and then covered by undeformed unit 60. The lower chronological constraint for BDT4-c is determined by the age of the youngest of the three detrital samples that we have dated (BDT4-41) from the gravels of unit 80, which can also be correlated with unit 80 in BDT3. This sample yielded a calendar date of A.D.1380–1430 (Table 4) indicating that event BDT4-c occurred after A.D. 1380. Event BDT4-d broke unit 100, a distinct silt and clay unit, and terminated below the gravels of unit 80.

[21] The age range of event BDT4-d is constrained by the ages of five newly dated charcoal samples (BDT4-10, BDT4-13, BDT4-44, BDT4-86, and BDT4-87) and two samples dated by GS94 (BDT4-66 and BDT4-84) from unit 100, two samples dated by GS94 (BDT4-57 and BDT4-53) from unit 105 (GS94 did not assign a name for this unit), a sample dated by GS94 from unit 110 (BDT4-76) and the age of unit 80 (Table 4). The resulting modeled age range for the earthquake is A.D. 1360–1425 (Figures 6c and 6d). Several fault traces which are interpreted to be associated with event BDT4-e terminate at unit 150. The modeled age range of event BDT4-e, A.D. 1285–1340 (Figure 6d), is constrained by the dates of four samples from different stratigraphic units that predate the deposition of unit 150 (BDT4-7, BDT4-20, BDT4-23, and BDT4-38). A sample dated by GS94 (BDT4-64) from unit 150 was also included in the earthquake BDT4-e age calculations.

3.3. BDT3

[22] In trench BDT3, the most recent earthquake (BDT3-a) that ruptured unit 80 is the A.D. 1857 earthquake (see

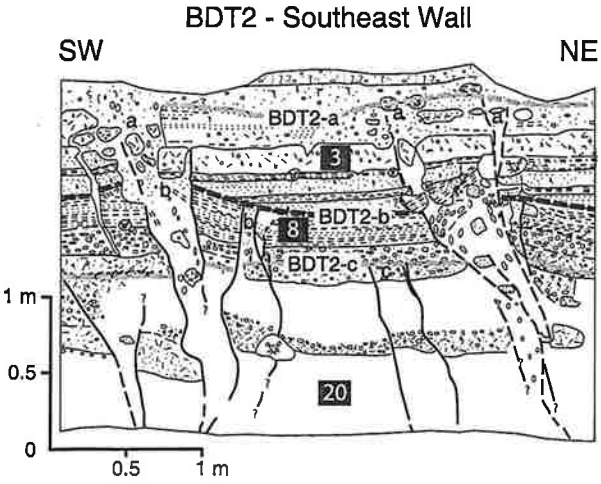

Figure 5. A portion of the southeast wall of BDT2 that display evidence for three events preserved at this trench (also see auxiliary material Figure S1). Fault strands are shown by heavy lines. Individual earthquakes are marked with small letters (a, b, c). Blank areas are fault zone breccia or bioturbated zones. Earthquake horizons are highlighted with thick dashed lines with different shades of gray for easy recognition and labeled as BDT2-a, BDT2-b, and BDT2-c. Two units that were dated in this study are labeled (units 3 and 8).

(3-1)

Stop 1, Day 3: **Wheeler Gorge submarine channel and turbidites**
Location: Highway 33 north of Ojai, CA

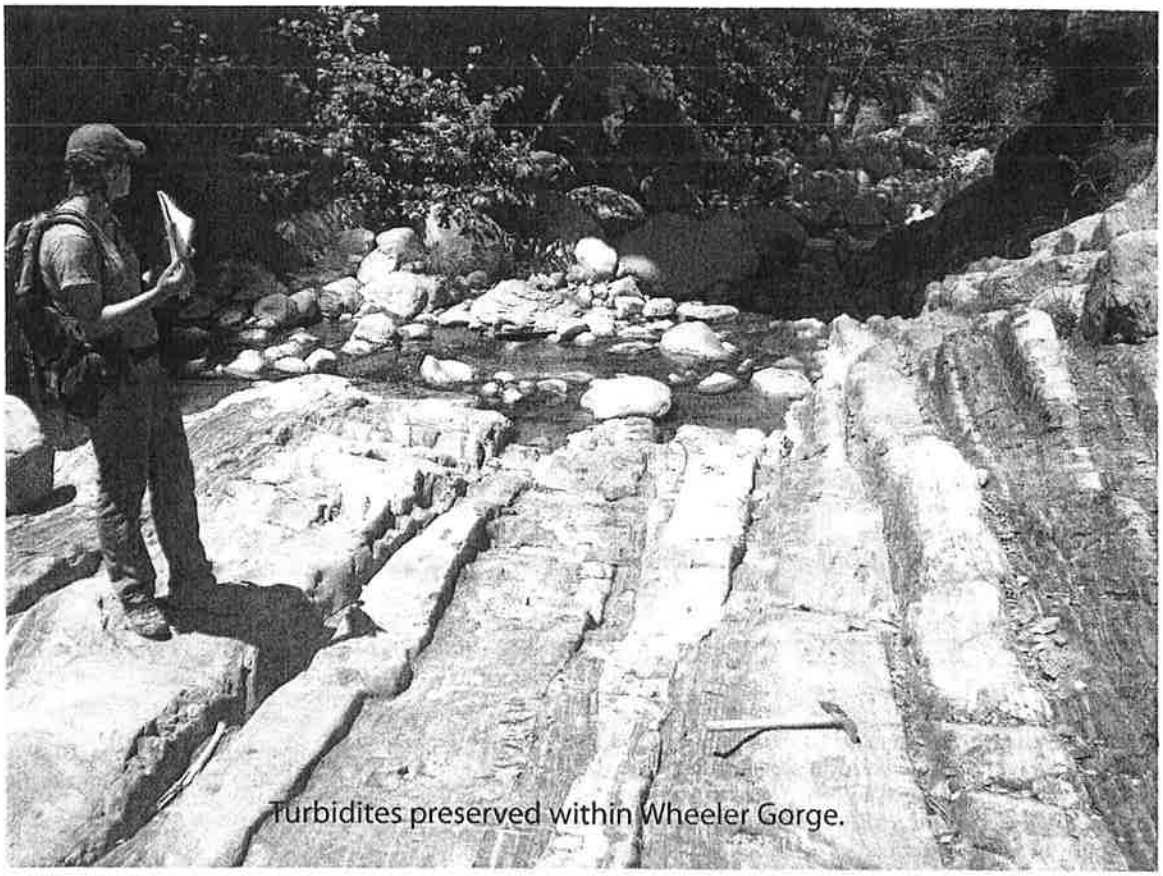

Turbidites preserved within Wheeler Gorge.

Overview (modified from Campion and Sullivan, 2009)

The trace of the Santa Ynez fault, which is traceable for more than 100 km, crosses the highway a short distance north of the northern tunnel. There, overturned to vertical, Cretaceous conglomerate and underlying black shale lie in fault contact with the Cozy Dell Fm. The stratigraphic separation along the Santa Ynez fault at this locality is estimated to be 2500-3000m.

The deep-water system at Wheeler Gorge is Cretaceous in age. A map and measured section through the gorge are shown on the following pages of this guide. These rocks have been interpreted as a levee-channel complex of a deep-water fan (Walker, 1985, 1992).

A variety of turbidite lithofacies can be observed in the gorge, including classic Bouma turbidites, cobble and pebble conglomerate, and course sandstone turbidites classified as S1 and Ss3 in Lowe's (1982) classification. Notice the variation in lithofacies as we walk through the gorge.

Overall, the section at Wheeler Gorge has been interpreted as a deep-water system based primariy on the turbidite lithofacies and on regional setting---forearc basin. In the most rectent interpretation of these rocks, the conglomerate and sandstone units were interpreted as the fill of a levee-channel complex. What has not been clearly resolved is the setting withn the basin --- basin floor or slope?

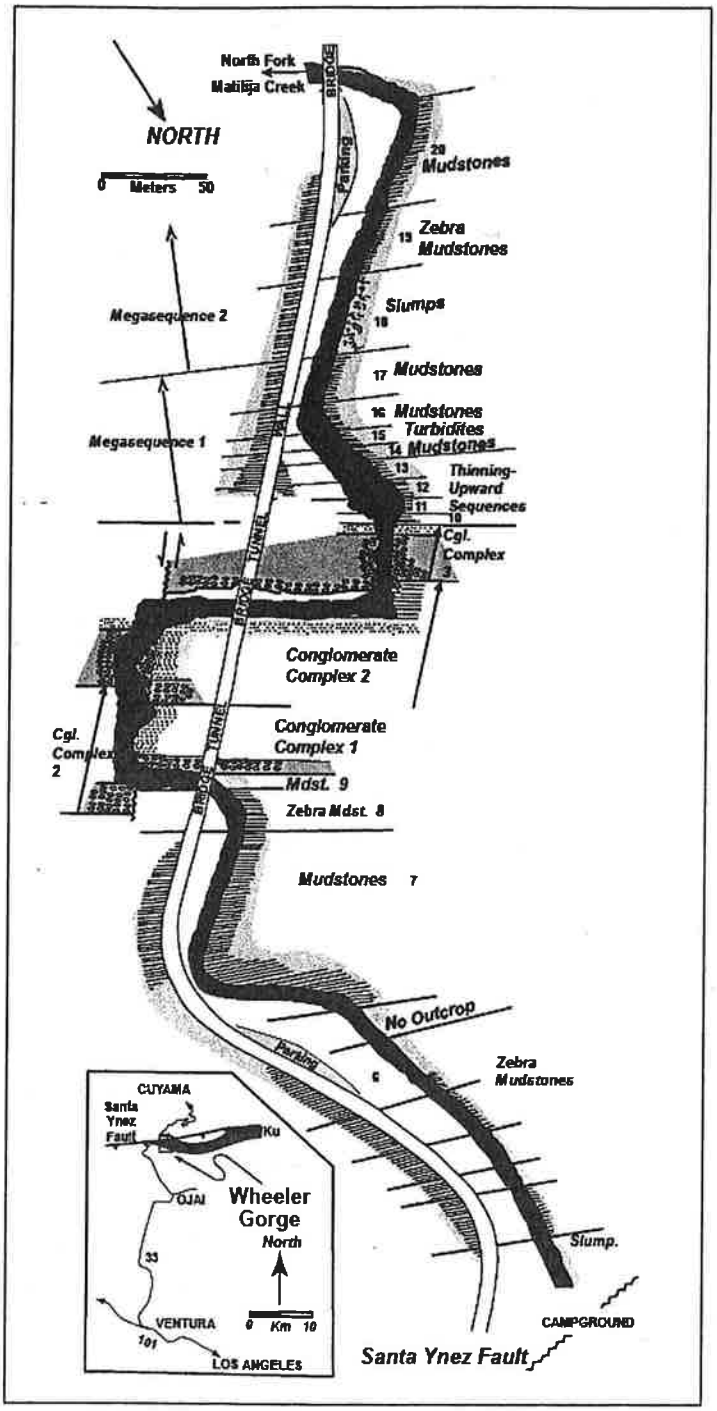

Map of submarine fan facies along Highway 33 at Wheeler Gorge. Outcrop is along the canyon walls of N. Fork Matilija Creek. Bedding dips steeply (70-90°) through the canyon. Numbers along edge of figure correspond to the stratigraphic column on the next page. Figure is from (Campion and Sullivan, 2009).

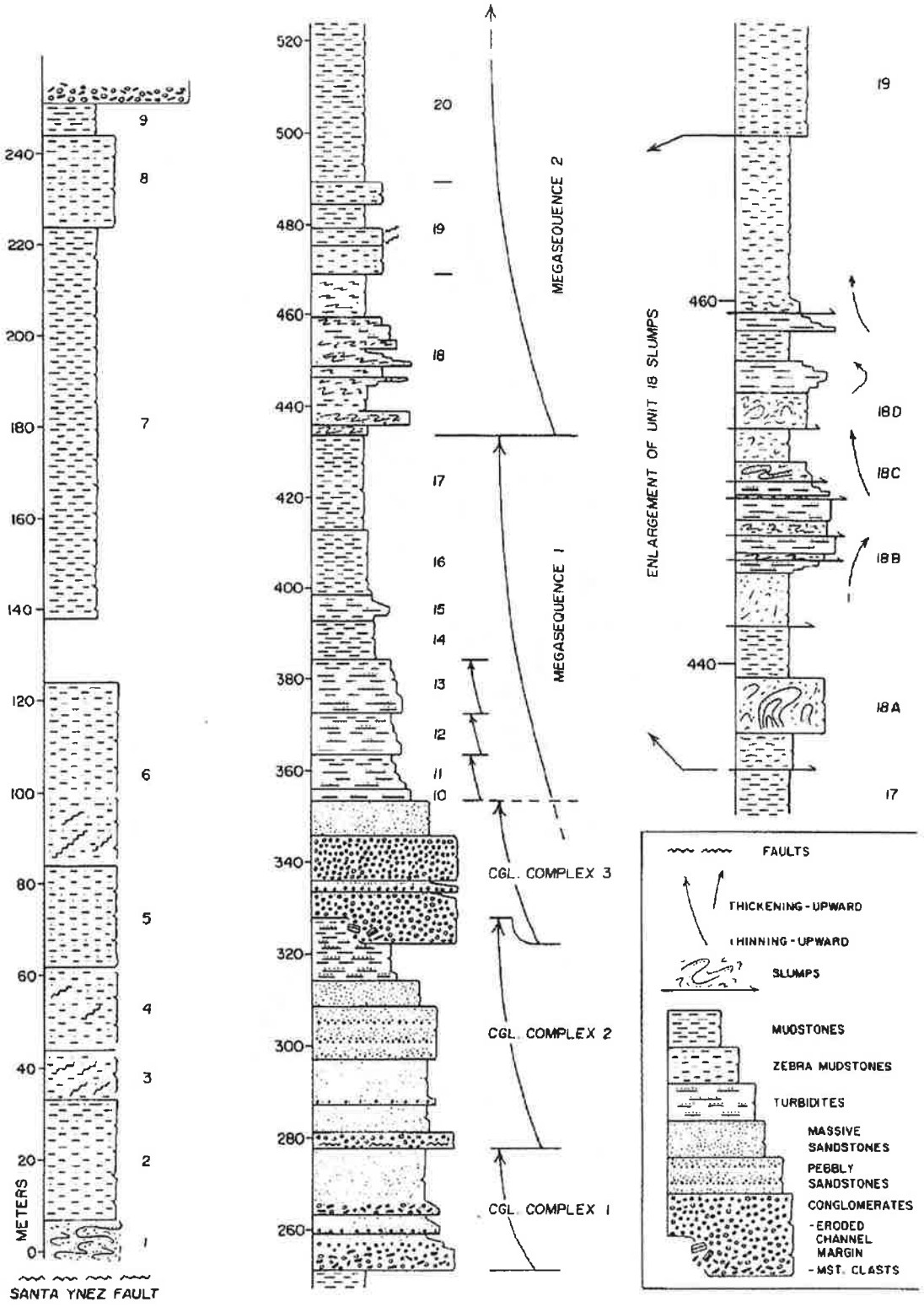

Figure 3 from Walker (1984) showing the complete measured section in Wheeler Gorge.

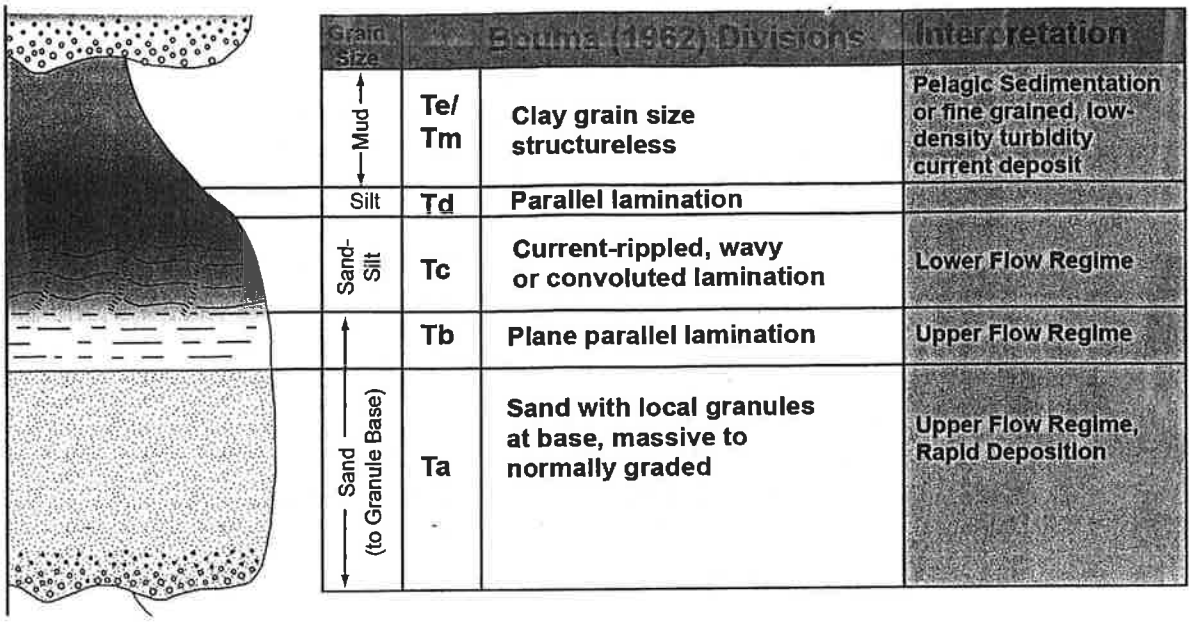

Idealized Bouma sequence (Ta-e) showing grain sizes, structures, and flow regimes. The complete turbidite is not typically deposited at any one location within the system, but different elements can be deposited at any one time. Thicknesses vary from millimeters to decimeters. Figure from Bouma (1962).

REFERENCES:

Bouma, A. H. (1962), Sedimentologoy of Some Flysch Deposits: Amsterdam, Elsevier, 168 p.

Campion, K. M. and M. D. Sullivan (2009). Cretaceous and Tertiary Deep-Water Systems in the Western Transverse Ranges, Southern California, AAPG Pacific Section Field Trip Guidebook, May 2, 2009.

Lowe, D. R. (1982), Sediment gravity flows: II. Depositional models with special reference to the deposits of high-density turbidity currents: J. Sed. Petrology 52, 279-297.

Walker, R. G. (1985), Mudstones and thin-bedded turbidites associated with the upper Cretaceaous Wheeler Gorge conglomerates, California: A possible channel-levee complex. Journal of Sedimentary Petrology 55, 279-290.

Walker, R. G. (1992), Turbidites and submarine fans: in Facies Models Response to Sea Level Change, Walker, R.G., and James, N.P, eds., Geological Society of Canada, 409 p.

Stop 2, Day 3: **Ventura River Terraces near Ojai, CA**
Location: Overlook along road near the east end of Casitas Reservoir

The Ojai Valley is located in the northwest corner of the Ventura Basin, and represents a tectonically active, intermontane valley deforming due to transpression south of the San Andreas Fault. The timing of deformation in the region is controversial, but likely has occurred within the last 2 Ma. Uplift along the southern margin may have initiated even later (0.2 Ma) based on the lack of Sulpher mountain detritus in Quaternary strata in the Ojai Valley (Ojai conglomerate).

Sub-parallel fault sets strike ~E-W through the region, and cut Quaternary terrace deposits. These river terraces represent the abandoned river floodplains that have now been uplifted and deformed due to active faulting and folding in the area. Rockwell et al. (1984) determined a ~39,000 year ^{14}C age for the strata below terrace Qt6a (see figure next page) and used this age to infer the ages of other terraces by extrapolating constant uplift rates over time. These terrace ages were then used to infer slip rates (0.3-1.0 mm/yr) on individual faults in the area. New cosmogenic ^{10}Be exposure ages on terrace boulders suggest a younger (<33 ka) age for the same surface, suggesting that either one technique is in error or that fault slip rates could be higher than previously determined.

PRELIMINARY QUATERNARY MAP OF THE OJAI VALLEY REGION

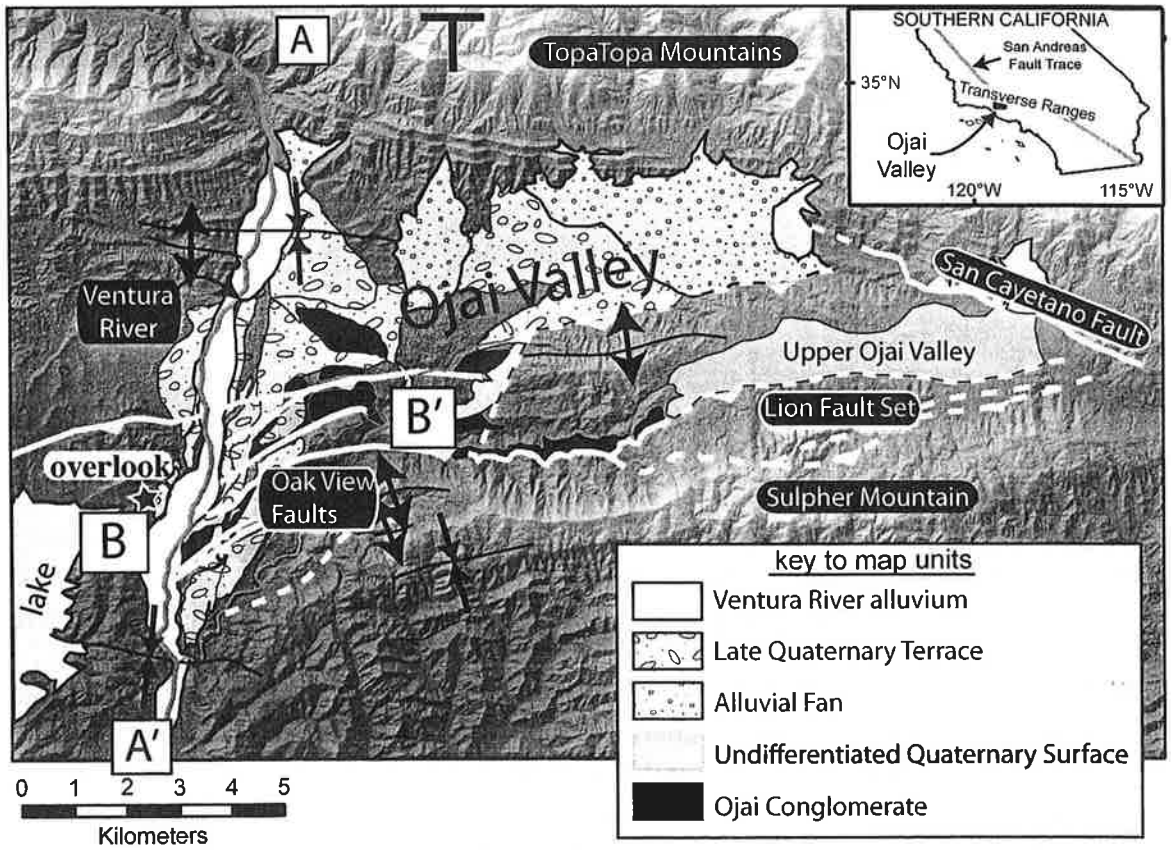

Quaternary map of the Ojai Region draped onto a shaded relief map of the area, modified after Rockwell et al. (1984) and Dibblee (1987).

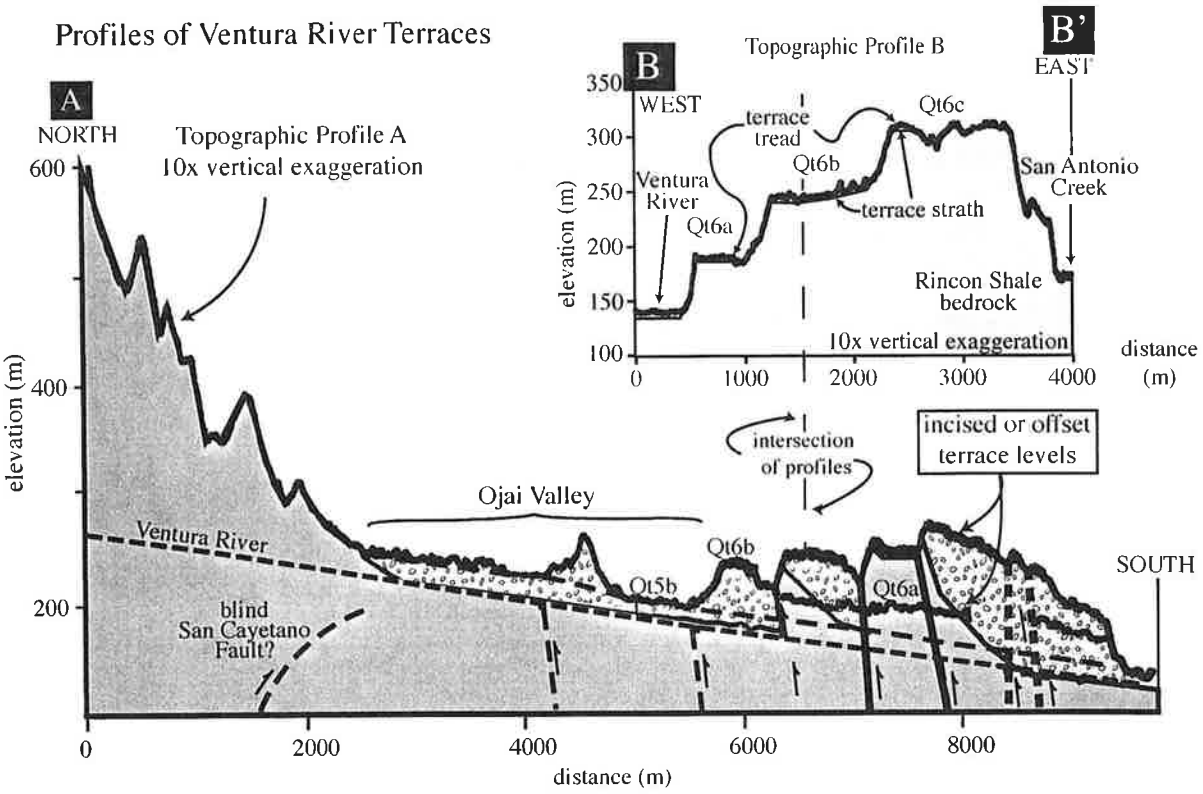

Ages and dating methods for river terraces near Ojai.

Terrace	Rockwell et al. (1984) age based on ^{14}C of Qt6a	Rockwell et al (1984) method	Heermance ages base on cosmogenic ^{10}Be exposure of Qt surfaces	Heermance cosmogenic method
Qt5b	30,000	extrapolation + soil	8,000±2000	depth profile
Qt6a	38,000	^{14}C	<33,000	6 boulder samples at surface
Qt6b	54,000±10,000	extrapolation + soil		
Qt6c	92,000±13,000	extrapolation + soil		

IMPLICATIONS

New cosmogenic ages indicate that slip rates may be 50-300% higher than previously determined. Why are new ages so different? What are the problems with each technique.

REFERENCES

Dibblee, T. (1987): "Geologic Map of the Ojai Quadrangle, California: Santa Barbara, CA," Thomas Wilson Dibblee, Jr. Geological Foundation, scale 1:24,000.

Rockwell, T. K., E. A. Keller, et al. (1984). "Chronology And Rates Of Faulting Of Ventura River Terraces, California." Geological Society Of America Bulletin 95(12): 1466-1474.